

02/2013

Title Story // Statistics on Structures 3.0
Shear Tests for Automotive Electronics
Surgical Modelling Simulation of Female Breast Reconstruction
FE-Model Calibration of a Railway Vehicle

RDO-JOURNAL

optiSlang

multiPlas

ETK

SoS

RANDOM FIELDS – KEY TO MODEL SPATIALLY CORRELATED UNCERTAINTIES

One of the most important trends in virtual prototyping is the investigation, optimization and proof of product robustness using CAE-based robustness evaluation, reliability analysis or robust design optimization. To achieve reliable results, all potentially influencing uncertainties, like manufacturing tolerances, material scatter or varying load conditions need to be taken into account by applying appropriate statistical definitions. But which discretization level of defining uncertainties is appropriate? Is it sufficient to define the uncertainties by using normal distributed single random variables neglecting any correlations between them? Is it sufficient to define correlations between single scattering variables? Or do we have to define the spatial correlation structure between scattering variables? Since the definition of uncertainties is the essential input to any stochastic analysis, these questions need to be discussed carefully for any engineering application. Anytime we realize that spatial correlations between scattering variables might have a significant influence and need to be taken into account, we need to model “random fields”.

During our last Weimar conferences, we discussed different approaches of “user defined” random fields using available CAD parameter to modify scattering geometry or using parametric functions to introduce some kind of “waviness” of spatial scattering variables. Both approaches to model random fields need intensive verifications that the resultant spatial correlated uncertainties represent what we intended to model: a realistic assumption of spatial correlation which we have seen at measurements.

Taking into consideration that there is an ultimate need to verify the resulting spatial correlated uncertainties by comparing them with measurements, the idea was born to use the “origin information” to automatically generate the random field parametric models instead of guessing or artificially creating them. Here, the “origin information” can be obtained from multiple real world measurements as well as from multiple realizations of a stochastic analysis of process simulation, like a robustness evaluation of a forming process representing the variation of the resultant product. After almost 10 years of methodology and software development for random fields, we successfully converged with our new software version Statistics on Structures 3.0 to offer user friendly and numerically efficient workflows to identify random field parametric models automatically. Please find more details in the title story of this journal.

Apart from that, in this journal, we have selected case studies about parameter identifications from different industries. I hope you will enjoy reading our magazine.

Yours sincerely



Johannes Will
Managing Director DYNARDO GmbH

Weimar, November 2013

CONTENT

2 // TITLE STORY // RANDOM FIELDS
Statistics on Structures 3.0

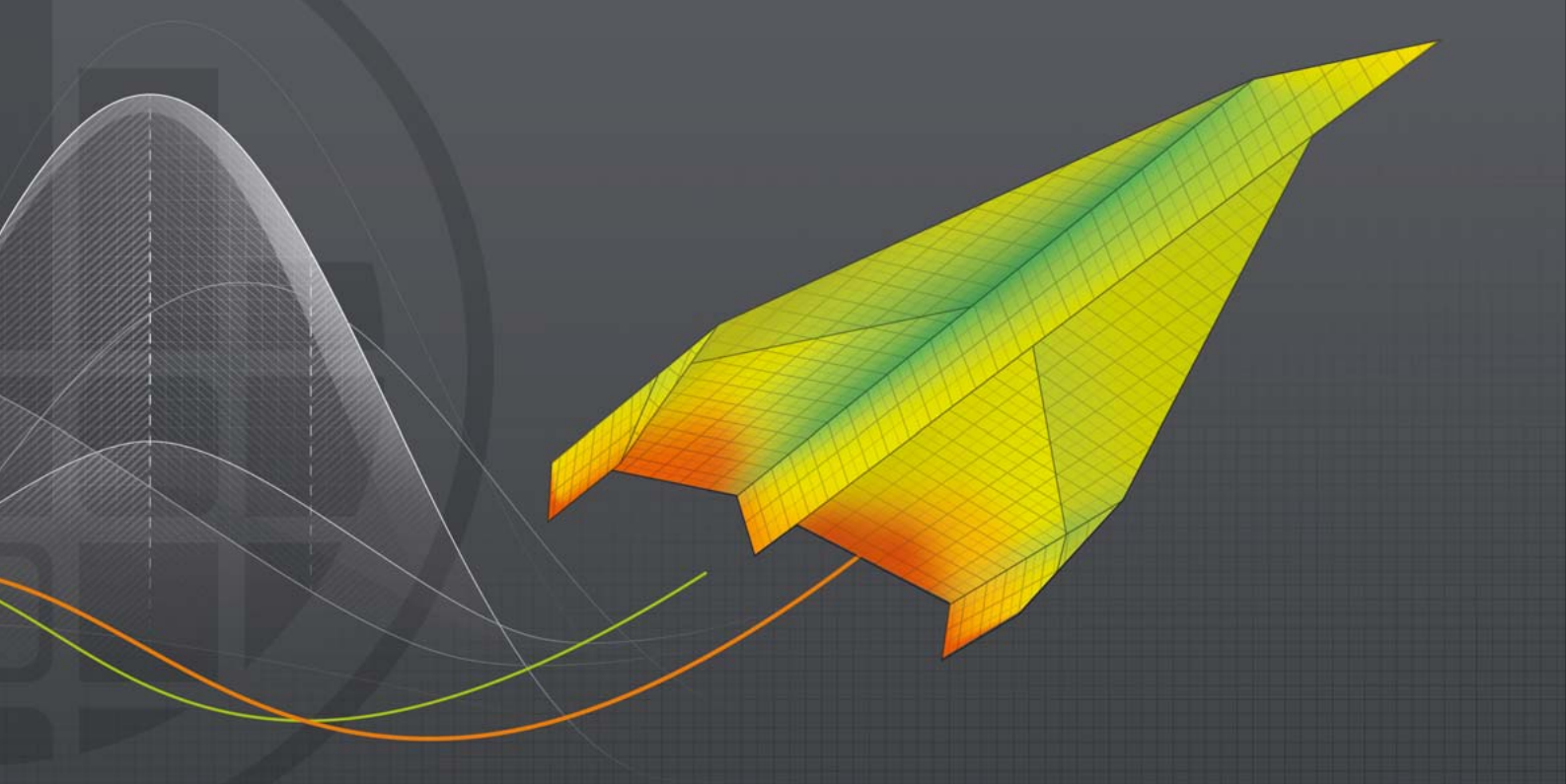
9 // CASE STUDY // AUTOMOTIVE INDUSTRY
Shear Tests for Automotive Electronics

14 // CASE STUDY // BIOMECHANICS
Optimization In the Planning Phase of Operations on the Female Breast

19 // CASE STUDY // RAILWAY INDUSTRY
Finite-Element Model Calibration of a Railway Vehicle

31 // OPTISLANG // METHOD OVERVIEW

32 // DYNARDO // SERVICE
Consulting, Support, Trainings



TITLE STORY // RANDOM FIELDS

STATISTICS ON STRUCTURES 3.0

Some properties of engineering structures or structural parts are usually of random nature due to manufacturing tolerances, material scatter or random loads. For the assurance of product quality, avoidance of recalls and fulfillment of safety requirements, such randomness has to be taken into account by applying correct statistical modeling. Statistics on Structures 3.0 makes random fields ready for CAE-based simulation.

Introduction:

Random variables vs. random fields

Random fields are not yet commonly used in CAE design. Probabilistic methods involving scalar random numbers, however, have experienced a success story in the recent years: They are used in a wide area from robustness evaluation, reliability analysis, robust design optimization, etc. In these areas, DYNARDO provides engineers optiSLang as one of the worldwide leading software tools. There is a wide acceptance among engineers that CAE-based stochastic analysis helps to obtain a more accurate representation of reality leading to better products with less manufacturing costs, better reliability and longer life-cycles. Nevertheless, most probabilistic procedures are currently restricted to individual random numbers, i.e. scalar parameters.

When applying CAE-based stochastic analysis to virtual prototyping, we have to learn what is the appropriate discretization level of the uncertainties, like we have learned and identified which is the appropriate accuracy level of spatial discretization (h/p/r-refinement, interpolation and integration types of finite elements) or the appropriate accuracy level of material constitutive models (linear, nonlinear, plas-

tic, creep, damage). Usually we start with rough estimations of uncertainties (for example, a uniform variation of a sheet metal thickness using one scalar stochastic parameter). Some phenomena, however, will require the introduction of spatially distributed random variations and here we will need random field parametric models in the future.

Random fields, i.e. random numbers being spatially distributed and obeying some spatial relationship, however, are currently very rarely used in CAE design and simulation. One reason is the conceptual difficulty of identifying and understanding. Another reason is the missing availability of numerically efficient and user friendly software solutions to identify and model random fields. DYNARDO's goal is to fill this gap with Statistics on Structures 3 introducing random fields in CAE design and analysis.

The assumption of scalar parameters is a very helpful view onto commonly used numerical models. Usually, the scalar output parameters are values being excerpted from scalar or even multi-dimensional fields. For example, in structural mechanics, one often extracts integral-weighted or maximum principal values (from stresses, equivalent plastic strains

or displacements) from fields being distributed among the nodes and elements of a finite element mesh. Even the input parameters are rarely truly scalar random numbers. For example, the shell thickness is never a constant for a single sample design in reality, but varies randomly among the finite element structure due to its manufacturing process. The same is true for the spatial distribution of geometric coordinates, material properties or boundary and loading conditions - all being randomly distributed among the FEM mesh. The parameterization and characterization of these random effects and, even more challenging, the identification of input-output relations are generally nearly impossible tasks when using element wise discretization of random properties since they may involve many thousands of random numbers. Spatially distributed random variables, however, can be characterized as random fields. Their description involves information on the distribution type, lower and upper bounds, mean value and standard deviation at each field position. Further, a correlation matrix between the individual field points describes the amount of fluctuation within the close neighborhood of an individual point: Usually a physical quantity (e.g. the shell thickness) does not change rapidly and the values of all nearby points are strongly correlated. The correlation matrix of a random field needs not necessarily to be computed, but can be approximated through the Karhunen-Loeve expansion.

Karhunen-Loeve expansion

The Karhunen-Loeve expansion states that an optimal choice of the basis functions is given by an eigenvalue (“spectral”) decomposition of the auto-covariance function. When a scalar field is measured as a distribution on an FEM mesh (or on any other discrete space), the random field is represented by discrete values. In this case the spectral decomposition is given through the solution of a (very large scale) matrix eigenvalue problem. A significant reduction in the number of variables can be achieved when truncating the series after a few items. The field being measured in terms of a large number of values (usually in terms of single values per node or finite element) is then expressed through a small number of coefficients (“amplitudes”). The “scatter shapes” (i.e. the eigenvectors of the covariance matrix) define the transformation basis. By reducing the number of random variables with the identification of the most important scatter shapes, we are then able to eliminate noise and simplify the representation of input/output relations, which will give us the possibility to visualize and understand the relation between input and output variation. The basis functions should be orthogonal reducing the computational effort for the projection (reduction) and its inverse transformation. As a side effect, the random coefficients are uncorrelated simplifying the digital simulation of random fields. The key aspect of the Karhunen-Loeve expansion is its reduction effect. That means one computes only a few scatter shapes in practice to explain the majority of variation. If the cumulative variability associated with the computed scatter

shapes is large enough, one is able to represent most of the existing variations in a random field using only a small number of scalar random variables. The omitted scatter shapes are usually associated with small correlation length parameters. Thus, they often can be considered as noise. Hence, one can interpret the truncated Karhunen-Loeve expansion in terms of

- model order reduction, breaking down the number of random variables of a complete field to a small number of random amplitudes. These amplitudes may be visualized and directly used in optiSLang’s sensitivity analysis using Metamodel of Optimal Prognosis (MoP) to determine input-output relations and the corresponding coefficient of prognosis (CoP).
- noise reduction and smoothing, eliminating random effects associated with very small correlation lengths. Such effects may, for example, be introduced by solver noise.



Fig. 1: New feature: Compute local error due to Karhunen-Loeve expansion (top) scaled to the dimension of the standard deviation. The respective standard deviation is shown on the bottom. The expansion uses 10 modes explaining 71% total variability. The local error can be directly related to the standard deviation enabling the engineer to predict the maximum error in variation at hot spots.

In order to validate the series truncation, one may use several error measures: A global error criterion that is related to the sum of the eigenvalues (being associated with the

actually computed scatter shapes) of the spatial covariance matrix. This global criterion provides a scalar number for the total variability percentage that can be explained by the reduced model. A local error (see Fig. 1, previous page) describes the amount of standard deviation that is lost when approximating the original data by the reduced model (see Fig. 2). If this local error is large in areas where the engineer is interested in, one must perform a detailed analysis: First, one computes the smoothed approximations to all field samples utilizing the scatter shapes. Second, one computes the minimum and maximum values and the standard deviation for all field values of the smoothed space. These quantities are then compared to their equivalents of the original data. Finally, one can determine how good the truncated Karhunen-Loeve expansion can represent extremal values and points of large variation.

Statistics on Structures (SoS)

DYNARDO developed the software Statistics on Structures (SoS) which is capable of decomposing random fields by Karhunen-Loeve expansion, visualizing the identified “scatter shapes”, analyzing random properties on FEM structures, locating “hot spots” of variation and investigating correlations. So far, SoS was mainly a “post processor” for statistics on FEM structures, i.e. for visualization of the descriptive statistics on the structure, visualization of correlations between random input and structural results, visualization of quality performance (QCS). To investigate the nonlinear correlation structure between input and outputs, SoS can be coupled with optiSLang. It can read and write optiSLang binary files integrating optiSLang’s MoP solver easily into the analysis of correlation.

Several successful applications of SoS are documented in the DYNARDO online library at www.dynardo.at and in the references at the end of this article. At the user conference WOST 2012, DYNARDO presented a new methodology for the analysis of random fields that was capable of analyzing very effective large finite element meshes (tested up to a range of 500.000). To meet future challenges in random field identification, the post and pre processing modes of Statistics on Structures were completely rewritten. Thus, computational efficiency and flexible work flows for user friendliness were improved opening new areas of application.

Using SoS for post processing of statistical data

Very often, engineers are interested in response value variation as a result of a robustness evaluation which must be evaluated at a mesh position of interest (“hot spot”) that is not known before starting the actual analysis.

An example shall explain the problem (see Fig. 3): One wants to investigate the variation and the correlation to the maximum von Mises stress within the structure subject to pre-

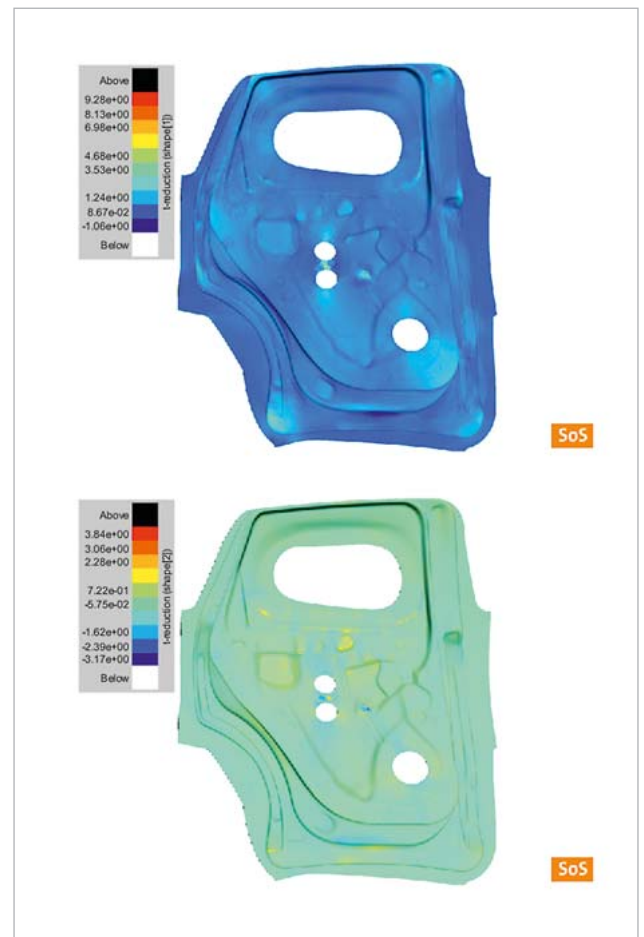


Fig. 2: The first two scatter shapes (scaled to the magnitude of the standard deviation) are shown in this figure (top: #1, bottom: #2).

defined material and process variation of a forming simulation. The engineer starts the task by performing a robustness evaluation varying all possibly influencing scattering parameters. This sampling is a necessary step to identify the hot spot of maximum stress and maximum largest stress variation. But how should the engineer express this quantity?

1. The challenge is that the position is a priori not known, where the largest stress appears or where the largest variations of the maximum stress can be expressed for the simulated designs. One choice is to perform a single simulation with representative design parameters, find the position of the maximum stress and choose this position to evaluate the variation for each design. But after performing the whole sampling, the engineers might understand that they evaluated the stress at the wrong position. This may involve a recomputation of the sampling doubling the amount of time and computational resources. The engineers may not even notice that they measured the stress at the wrong position and continues the analysis based on wrong data.
2. Another strategy is not to predefine the position of interest, but to extract the maximum stress from the complete mesh. This case may involve two types of

problems: First of all, the maximum stress may be measured at very different positions. If the maximas at different locations belong to different mechanisms the statistical significance of the correlation structure suffer (reduced coefficients of prognosis (CoP) when performing a correlation analysis including reduced ability to identify the important parameters). Even worse, one may extract the wrong values. For example, the maximum stresses may be measured near the supports. In this case one must carefully restrict the spatial domain where one extracts the maximum value from.

3. A third strategy is to evaluate integral values, e.g. one computes a weighted average of the von Mises stress. But this quantity might not represent extremal values well.

value on the mesh. By using the Karhunen-Loeve expansion to decompose the variation into the most important “scatter shapes”, one can easily cumulate the related amount of variation (being distributed on the mesh) into scalar parameters. The actual amount of variability related to the total field variance can be quantified. Hence, one can safely export the new scalar quantities to continue the sensitivity analysis. By analyzing the amplitudes of a truncated Karhunen Loeve expansion, one can increase the statistical significance, identify important input parameters influencing the individual amplitudes of the scatter shapes and even localize the effect for the respective inputs on the FEM mesh.

Let the task be: Identify the input parameters that dominantly influence a field quantity. The involved steps are sketched in Fig. 4. Let optiSLang generate a sampling and



Fig. 3: Finding hot spots with optiSLang and SoS

Statistics on Structures allows to define hot spots after performing the sampling (see Fig. 3). This gives much more freedom of choice to the engineer. Thus, it can simply be checked what is the most appropriate way of extracting results which represent all important hot spots of variation and show high CoP values of the correlation between input and the response. First, the engineer creates the sampling (using optiSLang or another software) and performs the numerical analysis of the robustness evaluation of the respective designs. Then the resulting field quantities (for example, the von Mises stress field) are imported into Statistics on Structures for all designs. Depending on the actual task, one can compute the statistical properties of the response values of interest. The positions of interest can then be identified in a post processing step. The values of interest at these positions are then exported as scalar parameters and can be further analyzed, for example in a sensitivity analysis of optiSLang.

perform the numerical analysis of each design. The resulting field quantity is imported into SoS for all analyzed designs. Therein, the random field is expanded and SoS computes the most relevant amplitudes (statistically independent scalar random parameters) and the associated scatter shapes for each amplitude (quantifying and localizing the amount of scatter related to the amplitude). In many applications, the scatter shapes can be successfully computed. For example, the mechanisms of variation can be decoupled and the varia-

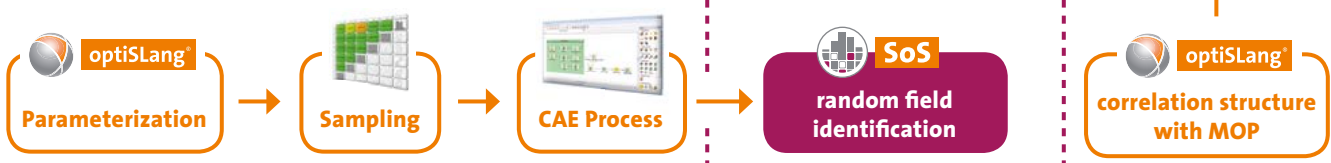


Fig. 4: Identify input-output relations using optiSLang and SoS

As mentioned, the selection of extreme values may lead to problems identifying the input/output correlation with large coefficient of prognosis when the extraction of the maxima involves rapid changes to the position of the considered

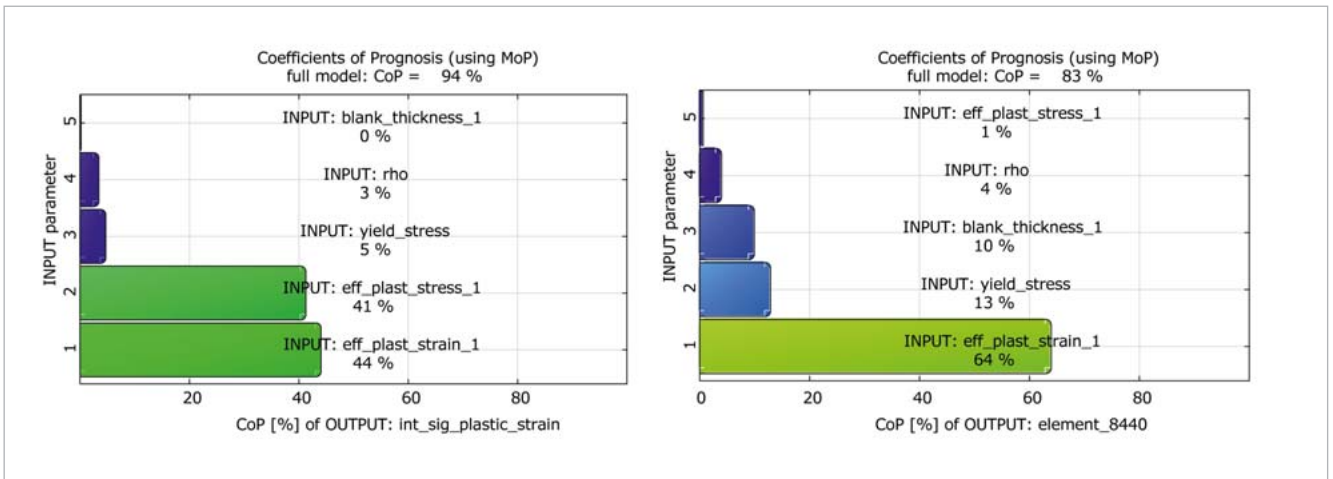


Fig. 5: CoP of the integral value of the plastic strain (left) or the CoP of an a priori specified element (element #8440 with largest plastic strain the the first design

tions are not too much affected by numerical errors. In these cases, the cumulative explainable variability in terms of CoP values should not be less than 90%. Ideally, only a few (3 to 5) amplitudes are needed to match this variability. The local error distribution should be validated in the post processing of SoS (see page 3). The amplitude samples are then exported to optiSLang. In optiSLang, the sensitivity analysis is carried

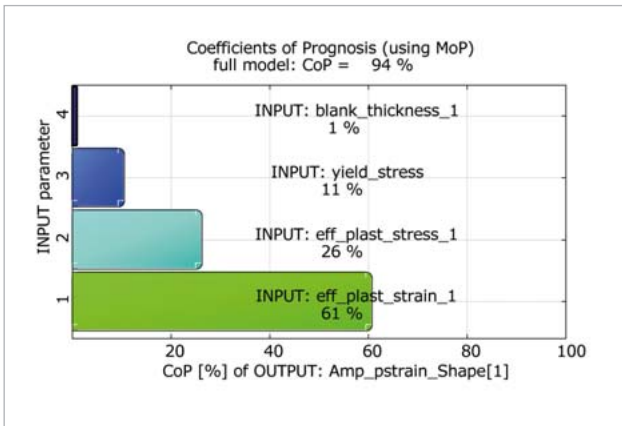


Fig. 6: CoP for the individual input parameters that influence the first amplitude of the Karhunen-Loeve expansion (45% of total variability in the model)

out for the original input parameters and the individual amplitudes (as outputs) using MoP. When interpreting the individual CoP, one must relate them to the amount of variability being associated with the respective amplitude. Further, one can quantify the position of the influence using the respective scatter shape.

The advantage of analyzing random field amplitudes compared with analyzing other scalar values is shown in figures 5 and 6: In figure 5, the overall CoP of a single element value might be too small for a useful interpretation. The integral average value (figure 5) is not sensitive to the yield stress although the response is (see the CoP of the amplitude in figure 6).

Using SoS for generation of imperfect sample sets using random fields

One of the main reasons of recoding SoS was to use the identified scatter shapes and amplitudes which represent the best possible parametric representation of spatially distributed quantities, for example shell thickness in sheet metal forming or bounding surface coordinates to generate imperfect sample sets. If the performance of a part having these spatial correlated scattering values after the forming process will be investigated in an assembly for a crashworthiness, it might become necessary to introduce the identified parameters in the robustness evaluation of the crash load case. In fact, the random field parametric model represents all information where each point on the mesh is a random variable being spatially correlated to the other mesh points. If the correlation structure and the probability distribution of the quantity are known, one can generate a sample of such a random field. Simulating a set of imperfect designs (involving multiple realizations of the same random field), thus, improves the accuracy of the representation of variations in reality.

Fig. 7 illustrates the procedure involving two steps: The first step is required to identify the random fields. Therein, one assumes that a random field quantity to be simulated, for example the shell thickness, is an output of a robustness evaluation of the forming process. A sampling is performed. For each design, the resulting field data are imported into SoS. A subsequent Karhunen-Loeve expansion analyzes the correlation structure and also identifies the scatter shapes and the related amplitudes. The random field parametric model necessary for generating imperfect geometries having the statistical representation of variation seen in the robustness evaluation of the forming process is being stored. In the following solver run (e.g. a robustness evaluation of crashworthiness simulation, or another manufacturing process like additional deep-drawing, welding, bending, folding, etc.) one then wants to introduce the scatter from the former process step, the spatially distributed shell thickness of the formed part using SoS random field parametric models.

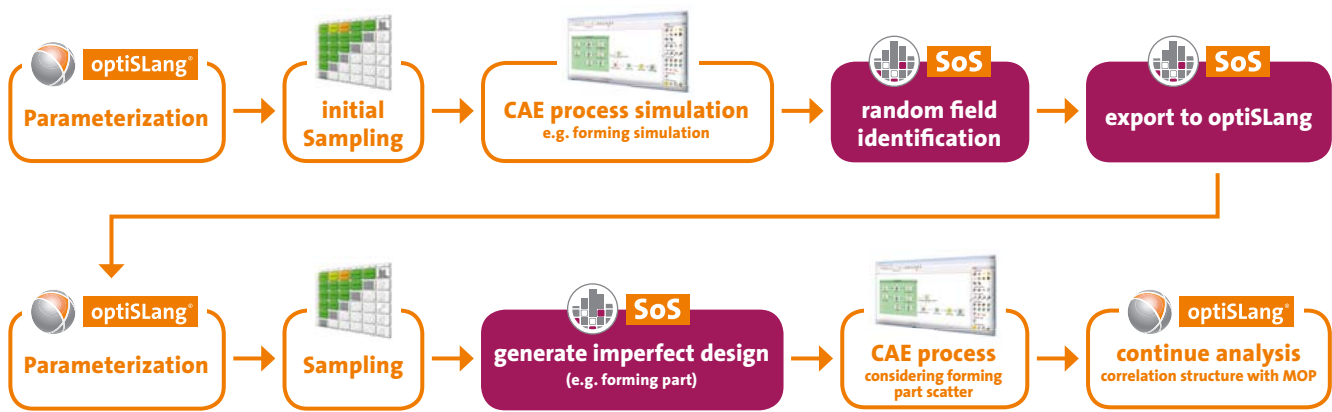


Fig. 7: Simulation of random fields using SoS and optiSLang

In optiSLang one parameterizes the problem involving both, scalar parameters and the random field parametric model imported from SoS. A sampling is created. Therein, optiSLang generates design directories for each sample. For each design directory it modifies all scalar parameters according to the parameterization. SoS is additionally called for each design reading the sample values of the amplitudes and generating imperfect realization of the formed part sheet metal thickness using the SoS random field parametric model.

Using SoS to eliminate random noise in a robustness evaluation

Noise is defined as a random perturbation at each mesh position which is statistically independent and has zero mean and finite variance. An extended interpretation used in SoS is to regard noise being a random perturbation which is not or negligibly correlated to the perturbation at other mesh positions. These variations are exactly those which are not part of the truncated Karhunen-Loeve basis. Hence, one can use the Karhunen-Loeve expansion to filter the noise from the computed field data samples. This is called “smoothing” (see Fig. 8). Smoothing can be used to filter random noise of those solver outputs being used as inputs in a subsequent simulation.

Detection of geometric deviations

A typical example of random fields are geometric perturbations. The geometry of a product is usually randomly perturbed due to random effects during the manufacturing process. Sometimes, for example in metal forming, it is possible to simulate the production process and to evaluate the geometric deviations after this step to reuse them as a random input in the next phase of the analysis of the production process. SoS supports the analysis by detecting geometric deviations (given a modified mesh and a reference mesh for the closest point projection), by analyzing and post-processing the correlation structure of the detected deviations by identifying shapes and amplitudes of deviation and by exporting the deviated geometry as input for a consecutive analysis.

The procedure is illustrated in Fig. 9 (see next page). In the example, a first CAE process simulates a production process, i.e. metal forming of a car cowling. The final geometry is randomly distributed due to random production parameters. A second CAE process is set up using the random geometry of the first process, i.e. a crash analysis, robustness analysis or a second production step. One usually sets up a single geometry and mesh. In order to apply randomly distributed geometries to the second CAE process, one has two

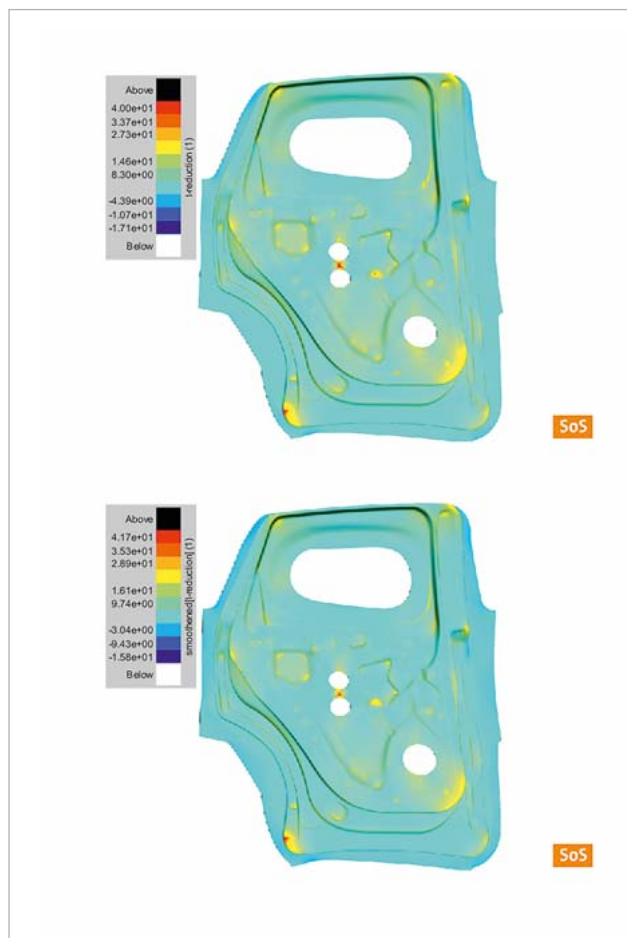


Fig. 8: The top figure illustrates a single design of the original data. The bottom figure plots the smoothed design (using the Karhunen-Loeve expansion with 10 scatter shapes, i.e. 71% variability)

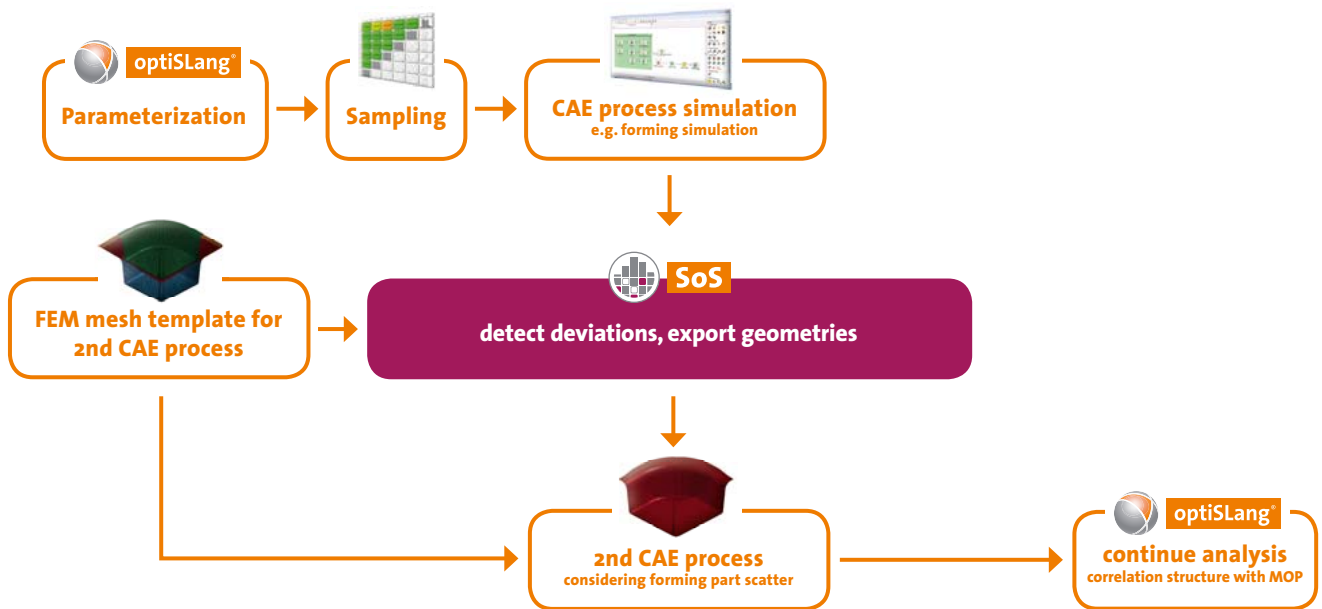


Fig. 9: Detection of geometric deviations and pre-process a consecutive analysis

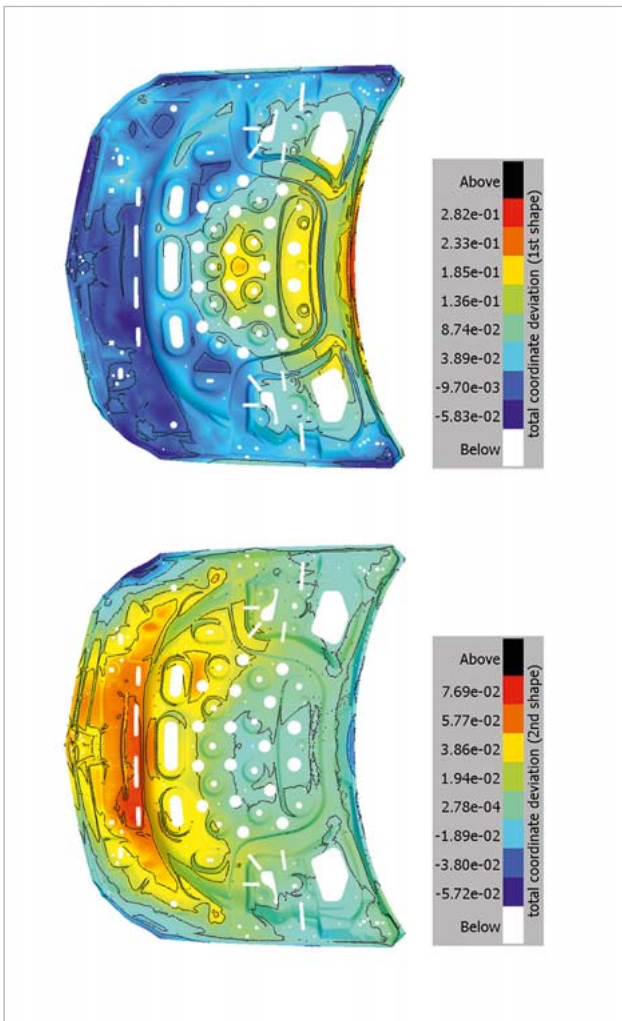


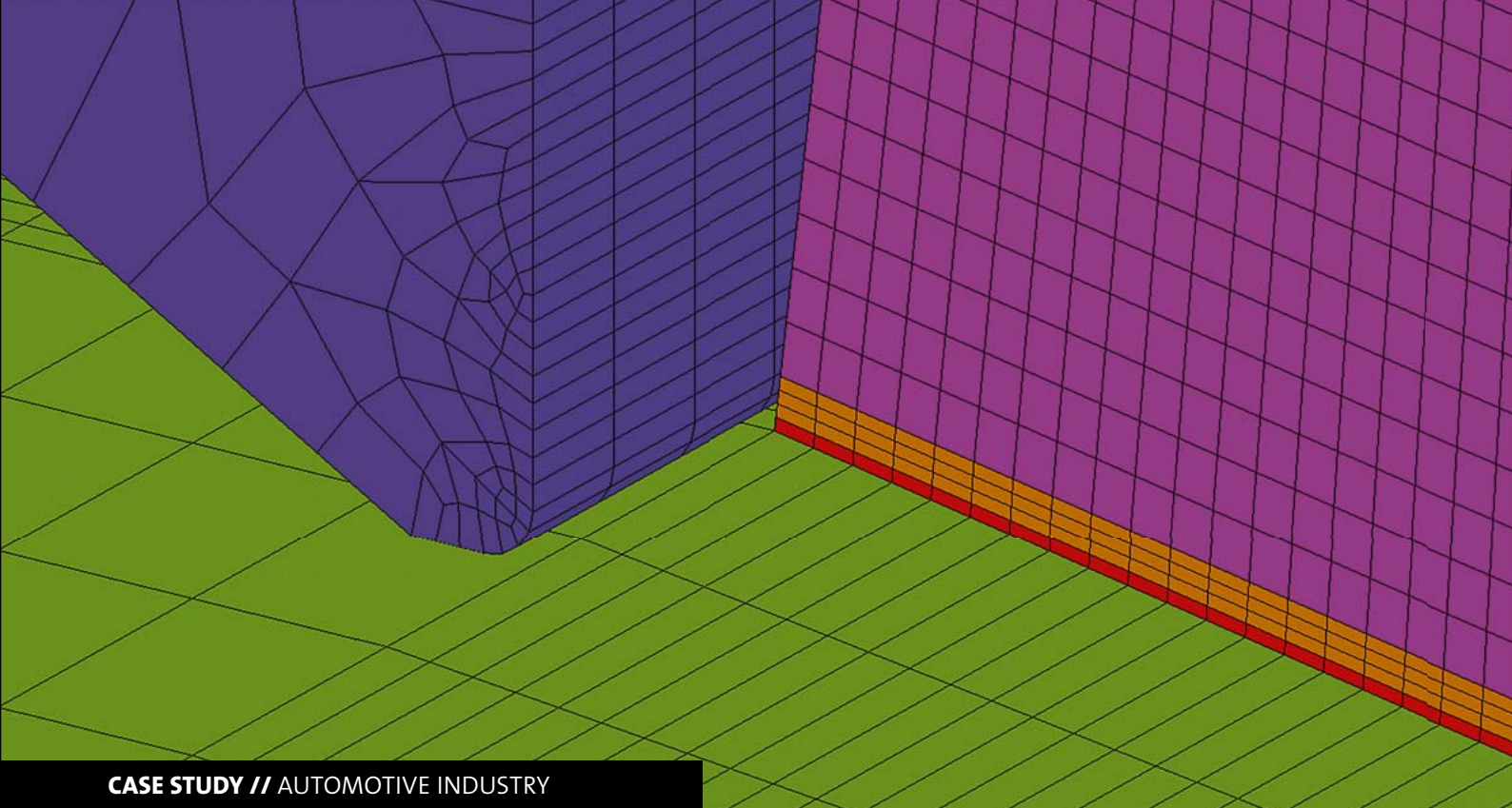
Fig. 10: Detection of geometric deviations between two incompatible meshes of a car cowling. Illustrated are the first 2 scatter shapes of the normal coordinate deviation explaining 90% of total variability.

choices: Either one detects the coordinate deviations between the final geometries of the first CAE process and the assumed model of the second CAE process to insert them directly as input geometries into the second solver chain. Or one detects the deviations and performs a Karhunen-Loeve expansion in order to generate the random input geometries for the second CAE process. Figure 10 illustrates the first scatter shapes of such coordinate deviations used in random field generation.

Authors // S. Wolff, Ch. Bucher (DYNARDO Austria GmbH), J. Will (DYNARDO GmbH)

Figures 1, 2 and 8 refer to the numerical example: Hansjörg Lehmkuhl, Johannes Will, Vera Sturm, and Jörg Gerlach. Which discretization level for uncertainties do we need for reliable robustness evaluations in forming application? In 9th Weimar Optimization and Stochastic Days, Weimar, Germany, 2012. DYNARDO GmbH. (courtesy of AUDI AG and Thyssen AG) Compared with this example, the images were created with SoS 3.0 demonstrating the new post processing capabilities of the new version.

Figure 10 is excerpted from: Will, J. Integration of CAE-based optimization and robustness evaluation in virtual prototyping processes at Daimler using optiSLang, Daimler EDM Forum, Stuttgart, 2013 (copyright/courtesy of DAIMLER AG).



CASE STUDY // AUTOMOTIVE INDUSTRY

SHEAR TESTS FOR AUTOMOTIVE ELECTRONICS

Conducting a Finite Element simulation and parameter identification, optiSLang and multiPlas are used for tests in the automotive industry to identify the shear and tensile strength parameters of the interface between mold compound and copper substrate.

Optimization task

The goal of the documented analysis was the buildup of an appropriate mechanical model and the parameter identification for the shear button test carried out at Bosch. The test has been performed at different hammer positions in order to identify the shear and tensile strength parameters of the interface between mold compound and copper substrate. For this purpose, nonlinear mechanical analyses with incremental loading up to the ultimate failure of the system were carried out.

To simulate the delamination of the interface as well as the cracking of the mold compound, the material library multiPlas was applied that uses multi-surface plasticity models at continuum element level. Besides the failure mechanisms of the interface, it was necessary to include the crack properties of the mold compound in the simulation model. The main reason was the appearance of a compression force component during the shear test that causes a high shear resistance of the interface and finally leads to failure of the mold compound. In other words, the shear test is not only a test of the interface strength, but rather a test of the mechanical strength of the mold compound. In addition, the contact modeling at the hammer tip has been found

as a key factor for a successful identification of the model parameters. Other than expected this is especially true for the high hammer positions and can be explained by a local stress resp. a local contact problem. Here, the strength properties of the mold compound also play an important role. Finally, a parameter set has been identified that allows for the fitting of all test shear forces. The fit parameters have been found to be very sensitive to changes especially of the contact model and the mesh density.

Goal of the analysis

The objective of the analysis performed is the identification of the model parameter for the recalculation of the delamination process between mold compound and Cu-substrate during the button shear test.

For this purpose the following data are available:

- geometric parameter of Cu-substrate, mold compound cone and shear hammer
- maximum shear forces and corresponding displacements for 10 different hammer positions at room temperature

and corresponding failure images showing the interface after the debonding of the mold compound from the Cu-substrate

The following questions are investigated:

- recalculation of the shear test at all available hammer positions
- identifying the failure mechanisms at the different hammer positions
- sensitivities of the interface parameter on the calculated shear forces
- identification of the material data which allow for the fitting of the maximum shear forces at low and high hammer positions.

The complexity of the developed model requires a large computational effort to calculate the failure load of the system and therefore the parameter identification was carried out by applying the Meta Model of Optimal Prognosis (MOP) feature of the optiSLang software. The identified data set was then recalculated by FEM to ensure the quality of the MOP. It has been found that the remaining difference between the solution based on the MOP and the FEM is within a $\pm 10\%$ band width.

Simulation Model

Figure 1 gives an overview of the structure. The structure has been analyzed by applying symmetry conditions in the XZ-plane and therefore in all figures only 1/2 of the model (Cu-substrate, mold compound and hammer) is shown. In Figure 2, exemplary two positions (lowest and highest) of the steel hammer are shown. From Figure 3, the detailed layered structure of the model can be seen. The red layer models the interface between Cu-substrate and mold compound (multiPlas – anisotropic joint with Mohr-Coulomb frictional law and softening). On top of the interface layer, three mold compound layers are assigned to an isotropic Mohr-Coulomb material (multiPlas – ideal plastic multi-layer joint) in order to model the fracture of the mold compound close to the interface. The applied Mohr-Coulomb material description of the interface is shown in principal in Figure 4. Figure 5 shows a typical shear stress distribution after initiation of the delamination process for one specific hammer position. The highest shear stresses appear at the location of the highest compressive stresses according to the applied Mohr-Coulomb frictional law.

Sensitivity Analysis

A sensitivity analysis was carried out with optiSLang to understand the main effects and most important parameters for the parameter identification. The input parameters are f_i (friction angle), coh (cohesion), ft (tensile strength), G_{I_fac} (mode I fracture energy factor) and G_{II_fac} (mode II fracture energy factor) of the interface material layer as well as $cntfric$ (contact friction between shear hammer and

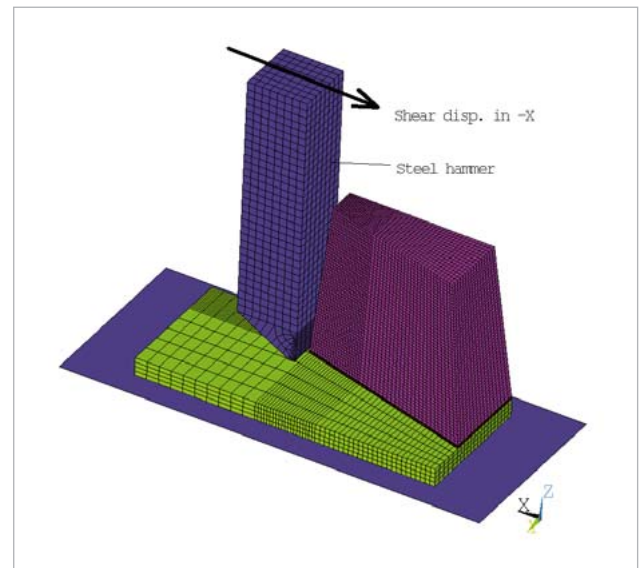


Fig. 1: Steel hammer with shearing direction

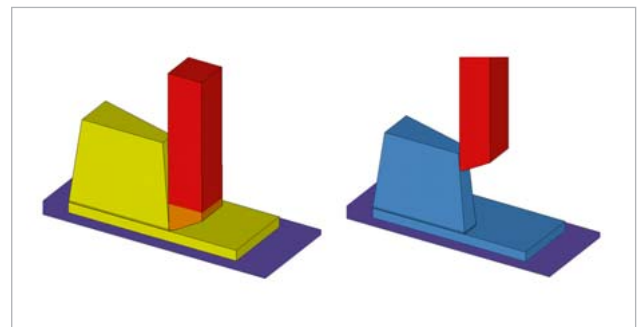


Fig. 2: Lowest and highest hammer position

mold compound cone) and $cnttmax$ (maximum contact shear stress between hammer and mold compound). The outputs are the maximum shear forces and corresponding displacements at all different hammer positions.

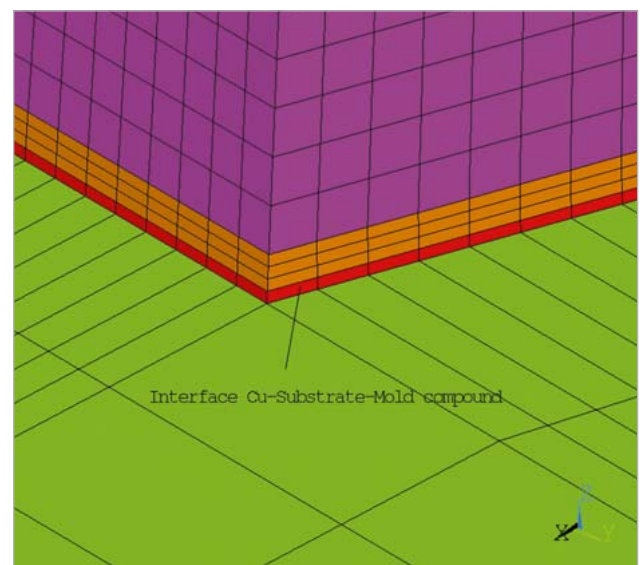


Fig. 3: Interface layer (cohesive zone)

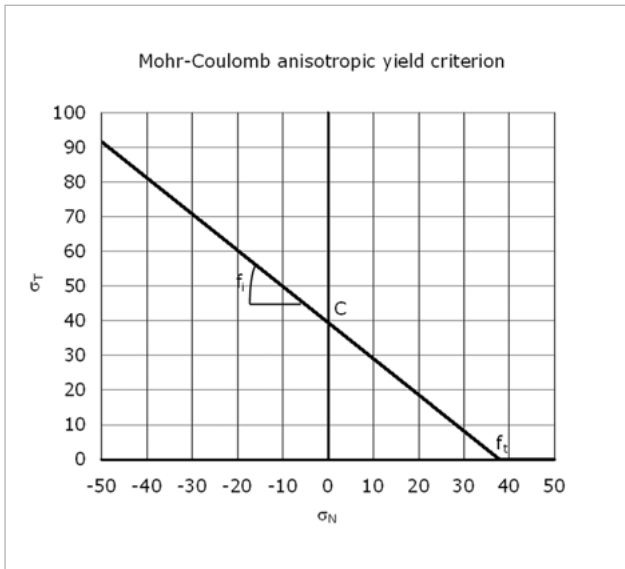


Fig. 4: Mohr-Coulomb frictional law (multiPlas Mat #120)

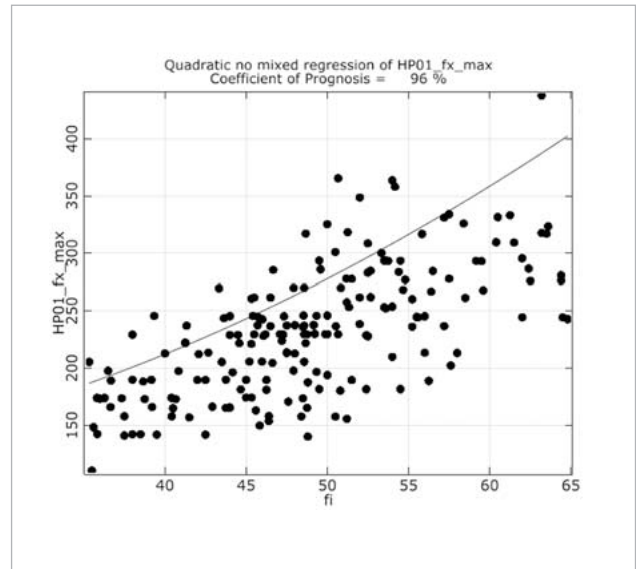


Fig. 7: Anthill plot – lowest hammer position

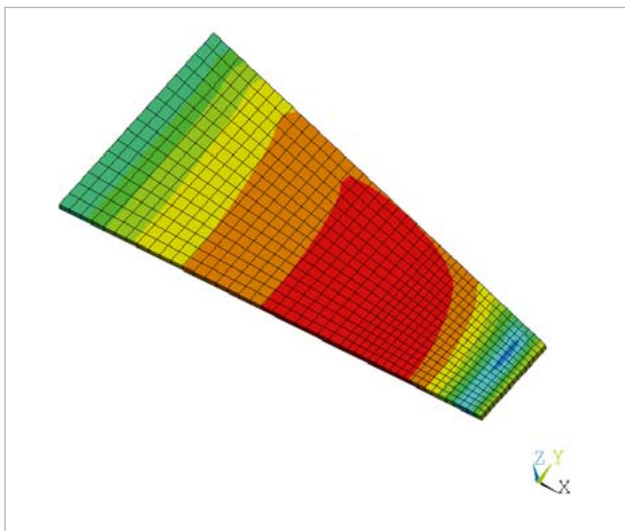


Fig. 5: Shear stress distribution in the interface layer

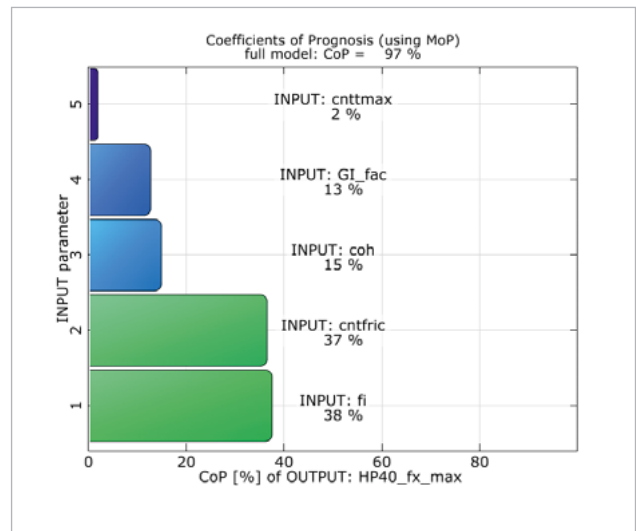


Figure 8: Coefficients of prognosis – highest hammer position

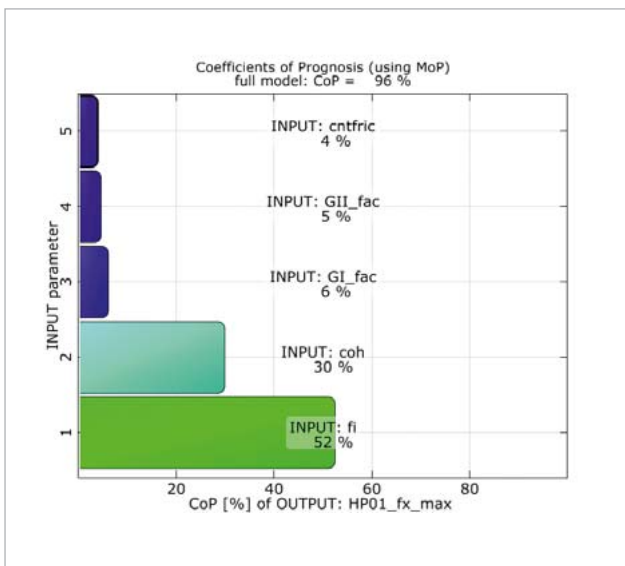


Fig. 6: Coefficients of prognosis – lowest hammer position

It has been found that at low and high hammer positions different parameters are of importance and complex mixed term regression models are needed to describe the systems behavior. In Figure 6 and Figure 8, the important parameters with their Coefficients of Prognosis (CoP) are shown for the lowest and highest hammer position. As an example, the Anthill plot of friction angle and maximum shear force at the lowest hammer position is shown in Figure 7. The MOP is based on 200 Latin Hyper Cube samples and total CoP values larger than 95% enable the use of the Meta Model in later optimization or identification tasks.

Parameter Identification

The identification of a unique parameter set which fits the simulation results to the experimental data for all different hammer positions has been performed by using the MOP-

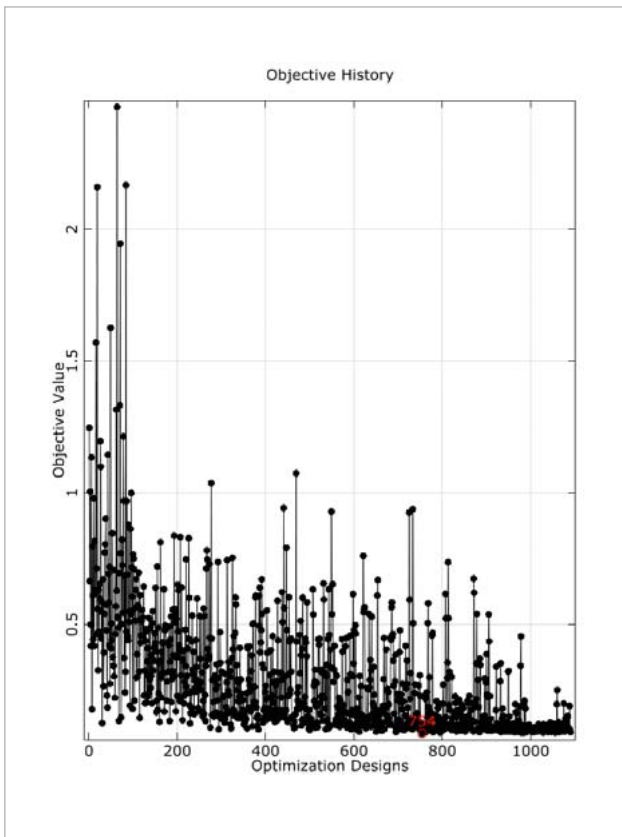


Fig. 9: Objective history global search

solver calls are used which require several hours or even days instead of a few seconds required by the MOP-Solver to approximate the solution based on a Meta model.

Figure 10 shows the comparison of the test and the simulation data. In addition, the recalculated results of a few designs by direct FEM-Solver calls are plotted in Figure 10. It has been found that the difference is about +/- 10% compared to the MOP-Solver approximation.

Conclusions

A finite element model has been developed that allows for the recalculation of all hammer positions in terms of maximum shear force F_{max} and displacement U_{max} using a unique set of material data for the button shear test. This could be achieved by applying the material library multiPlas for the interface and mold compound material to take into account multi-surface plasticity constitutive laws (anisotropic and isotropic Mohr-Coulomb and Drucker-Prager yield criterion). The Meta Model of optimal Prognosis (MOP) has been used to identify the important parameters and to fit the simulation model to the shear test data. This approach has been found to be most suitable for such noisy and time consuming non-linear simulation models.

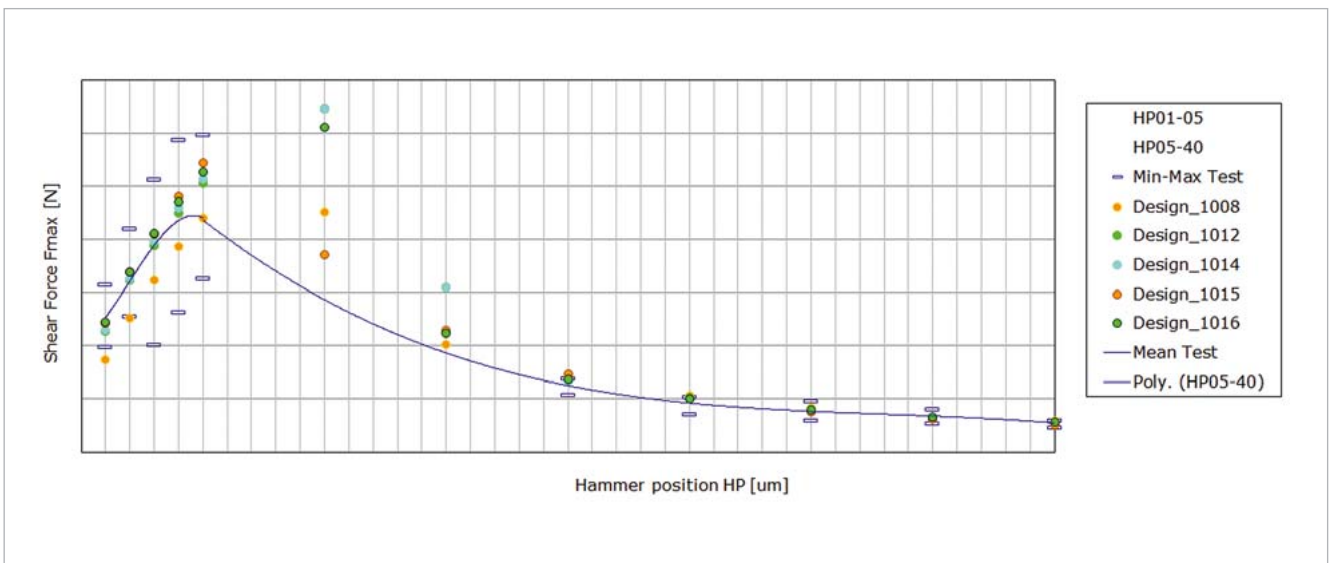


Fig. 10: Comparison of simulation and test results

Solver of optiSLang. Therefore no direct solver calls are necessary during the identification and the solvers noise resulting from the non-linear limit load calculation is smoothed out by the response surface approximation.

As optimization procedure a global evolutionary algorithm has been applied to avoid the convergence to local optima which fit only to specific hammer positions. In Figure 9 the history of this global search with more than 1000 realizations is shown. Of course this wouldn't be possible if direct

In general, it has to be mentioned that the Meta model itself (the response surface) is very complex due to the brittle softening of the materials and requires at least 200 DOE samples. Otherwise the nonlinear correlations of strength and energy parameters cannot be identified.

Authors // J. Gromala (Robert Bosch GmbH, Automotive Electronics) / A. Müller, R. Schlegel (DYNARDO GmbH)



ANNUAL WEIMAR OPTIMIZATION AND STOCHASTIC DAYS

DYNARDO's conference for CAE-based parametric optimization, stochastic analysis and Robust Design Optimization (RDO) in virtual product development.

Our annual conference aims at promoting the successful application of parametric optimization and CAE-based stochastic analysis in virtual product design. The conference offers focused information and training in practical seminars and interdisciplinary lectures. Users can talk about their experiences in parametric optimization, service providers present their new developments and scientific research institutions inform about state-of-the-art RDO methodology. We explicitly do not only invite optiSLang us-

ers as lecturers or participants, we also offer everyone who is interested in the topic a platform of exchange with acknowledged specialists from science and industry.

You will find more information and current dates at :
www.dynardo.de/en/wosd.

We are looking forward to welcoming you to the next Weimar Optimization and Stochastic Days.

OPTIMIZATION IN THE PLANNING PHASE OF OPERATIONS ON THE FEMALE BREAST

For the surgical constitutive modelling of the female breast, material parameters can be optimized using finite element simulation with optiSlang and ANSYS based on MRI data and 3-D surface scanning.

Optimization task

In the planning phase of operations on the female breast, e.g. breast reduction or breast reconstruction after tumour removal, surgeons usually have to rely solely on their experience acquired in previous procedures and their individual set of skills. Today, these interventions are commonly planned by manually drawing reference lines on the breast. Modern, computer-based planning tools have not yet found their way to the operating room. The benefit of these methods has been shown in other disciplines like engineering and physics, but still there is a lack of acceptance in the medical sector, especially when it comes to surgery planning. However there is remarkable potential for these computational methods in this field of application.

For an accurate planning of breast surgeries it is fundamental, to have sufficient understanding of the behaviour of the biological soft tissue under mechanical loading. For the simulation of the resulting deformations, numerical approaches such as the finite element analysis (FEA) are commonly used in mechanical and civil engineering. Even though numerous studies have been published to acquire material parameters with various material testing devices, yet no consensus could

be found nor on the theoretical models to be used to simulate the mechanical behaviour of the breast's soft tissue, nor on reliable magnitudes of parameters that describe its stiffness. Theoretical models range from simple linear elastic models over various hyper-elastic approaches, such as Neo-Hookean, Mooney-Rivlin or Ogden to visco-elastic formulations. In addition the stiffness which is described in literature for these tissues is not even always in comparable magnitudes: up to a factor of 30 lies between the softest and hardest material formulation that has been proposed, depending on the strain level. It is evident that there is further need for research on this subject.

Here, we want to introduce a method that takes advantage of the optimization algorithms provided by the software optiSlang to find the optimal set of material parameters for the mechanical modelling of the breast's soft tissue. The presented approach is applicable for different theoretical models and may deliver patient individual optimal material properties that may further be used as valuable input data for the simulation and planning of surgical interventions. For this procedure, a combination of magnetic resonance

imaging (MRI) and three-dimensional body surface scanning (3-D) together with finite element simulations with the software package ANSYS is used in an automated process chain. Material properties of the investigated tissues are used as design variables for parametric optimization loops on this process chain where simulation results are compared to the acquired patient individual imaging data.

Material and Methods

In contrast to other approaches that use tensile testing devices to create stress-strain relationships for the investigated biological materials the procedure which is described in this paper does not involve any real physical test on specimens. Instead it relies on two modern non-invasive imaging methods that do not require any contrast agents to acquire the necessary patient individual data.

Firstly, MRI imaging data is used to access the inner anatomy of the chest region of the test persons. However this imaging technique has the shortcoming that conventional MRI can only be performed for the patients lying horizontally in the tube. Though, open MRIs where patients can stand upright do exist, they are more expensive and by far less common compared to the standard horizontal MRI devices that are available in most hospitals.

Hence to acquire the standing positions a different technique was used: 3-D surface scanning. This bears the advantage of being relatively economically. With scanning devices that more and more leave the niche of expert applications and enter the consumer market, they can easily be afforded even for resident physicians in private practices. But of course these devices are only suited for the acquisition of the patients skin surface geometry and deliver no information about the underlying anatomical parts. Thus, a combination of both imaging modalities is still necessary. For the presented study, 3-D data derived from a collective of eight healthy female test persons was used.

3-D Surface Scanning

The imaging in upright position was performed using a surface scanner that uses laser triangulation technique (Konica Minolta Co., Ltd., Osaka, Japan). This system has largely shown its applicability to breast shape measurements in preliminary studies of the research group Computer Aided Plastic Surgery at Klinikum rechts der Isar in Munich. The 3D surface scans of the subjects were performed in standing position on predefined markers on the ground under standardized lighting conditions with the scanner facing the participants in +30, 0 and -30 degrees relative to the lens in standing position. The volunteers were asked to inhale and hold their breath for the time of the acquisition. The so produced data was processed in appropriate software (Geomagic Studio 12®, Raindrop Geomagic, Inc., NC, USA) to create one surface representation of each volunteer's chest.

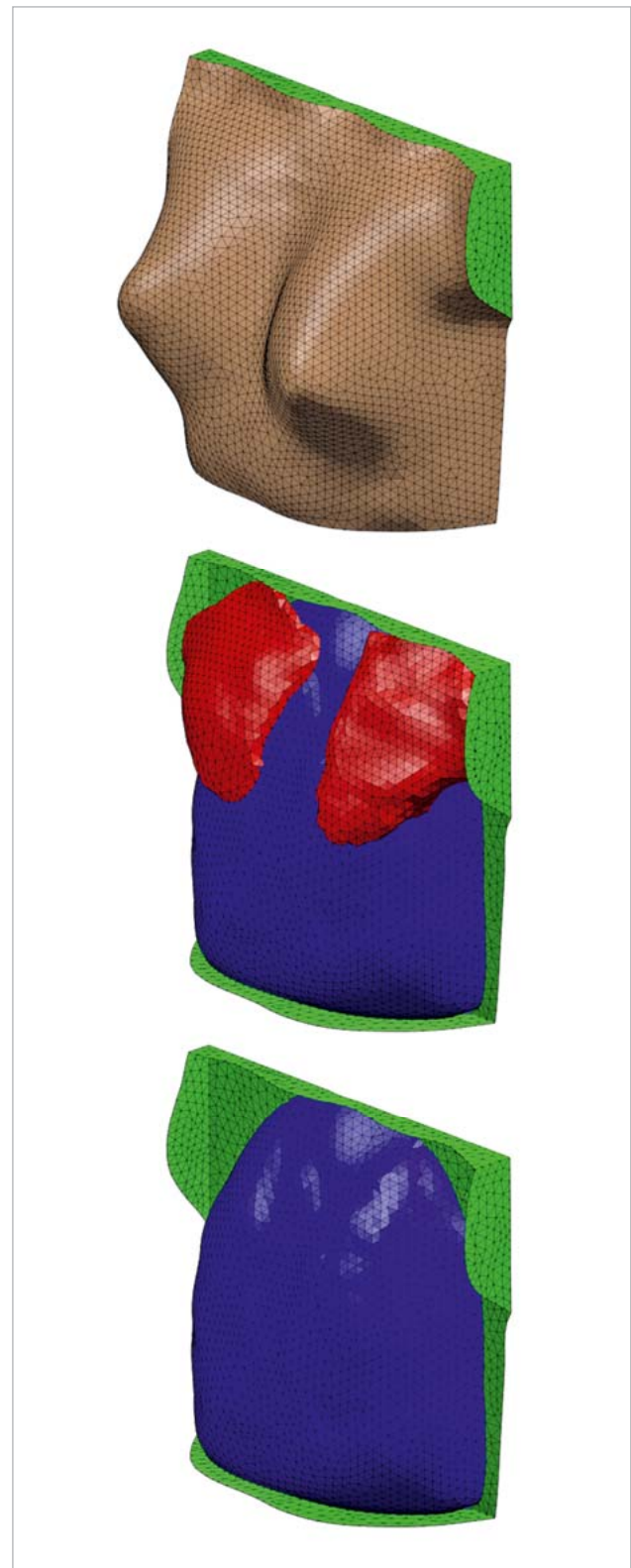


Fig. 1: Finite element models derived from segmentations of MRI data in prone position. Full body model (top), internal geometry of the pectoral muscles (middle), thoracic wall and fixed system boundaries (bottom)

Magnetic Resonance Imaging

Volumetric Magnetic Resonance Imaging (MRI) data of eight volunteers was acquired with the aid of a Philips Achieva 1.5 Tesla MRI scanner, using a spacing of 0.994 mm x 0.994 mm x 2 mm. The thoracic images were obtained

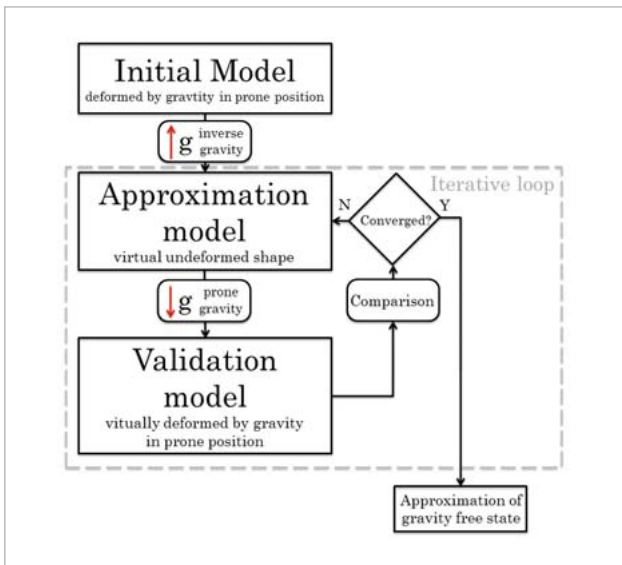


Fig. 2: Principle sketch of the iterative procedure for the approximation of the load free configuration.

with the participants lying in prone position. It was taken care that the breasts did not touch the bench, which was achieved by pillow support at the clavicle, neck and shoulder region as well as further down to the lower belly area and the pelvic crest region. However the breast soft tissue is not without deformed because gravity forces still act and cause a non-negligible deformation of the breast. Thus only the shape of the free hanging breast can be delivered for further processing in imaging software packages. The volumetric MRI data was segmented (used software: Mimics® 14.0, Materialise Inc., Leuven, Belgium) into different anatomical compartments and finite element models were derived out of this data.

Finite Element Simulations

Boundary conditions in the simulation were rigid fixation at the thoracic wall (i.e. the rib cage) and at the lateral system boundaries that have been defined by a standardized box around the region of interest of the simulation. In order to focus on the breast soft tissue behaviour solely, in the here used modelling the muscular tissue has been approximated to be rigidly fixed as well. An example for a utilized finite element mesh including the system boundaries is shown in figure 1. The theoretical material model that has been used in this particular study was the hyper-elastic Neo-Hookean formulation.

Iterative inverse calculations

As previously mentioned the starting configurations of the models that are based on MRI images taken in prone positions may not directly be used for finite element simulations because of the unknown initial deformation due to gravity. Due to the soft constitution of the tissue, the breast is highly deformed even if besides gravity no other forces are acting. But for mechanical simulations, an unloaded state of the geometries has to be known to be used as the starting geometry by the simulation. Calculating the non deformed reference state out of a known deformed configuration can be classified as an inverse problem. Due to the high deformation and the hyper-elastic material behavior, a simple, one-step inverse calculation with inversed gravity loading is not satisfyingly accurate. To address this issue in this work, a heuristic approach has been used and has been implemented in ANSYS APDL. This procedure is capable of calculating a stress free representative of the model based on a geometry which has been acquired under gravitational loading. The principle workflow of the method is shown in figure 2.

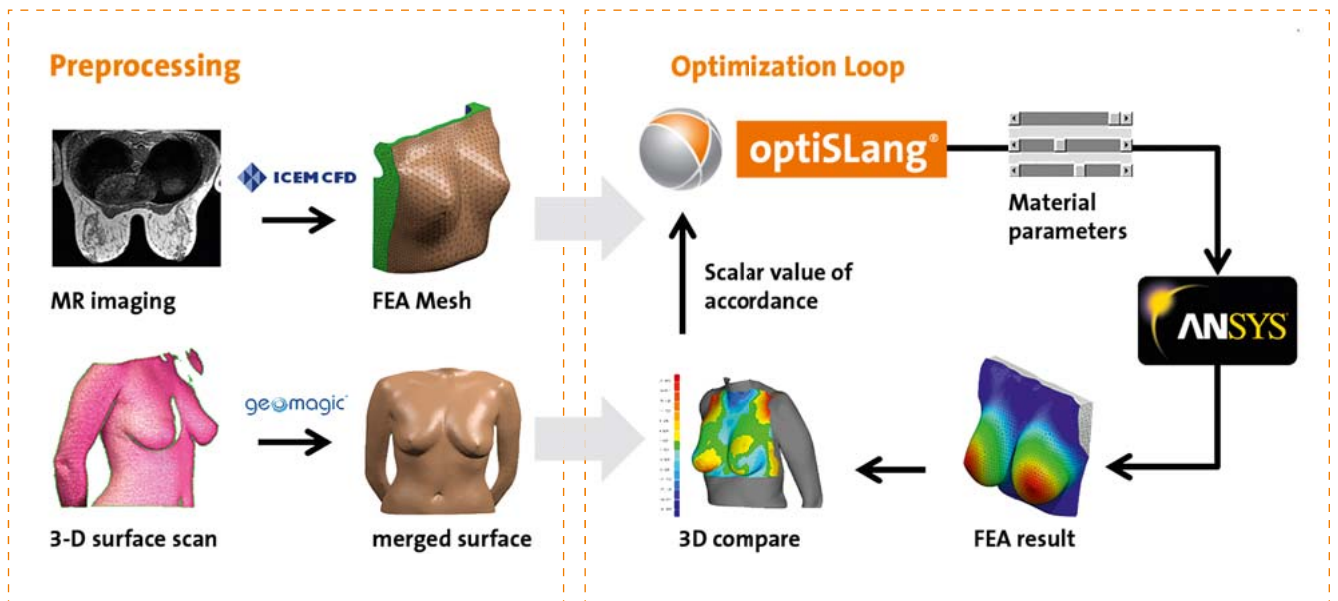


Figure 3: Principle workflow of the whole approach. The ANSYS calculation includes the iterative procedure visualized in Fig. 2.

This inverse procedure delivers an approximation of the stress free geometry of the breast. This model may be used for further simulations of different loading scenarios, while in the present workflow it is used to calculate the breast geometry in upright standing position.

Optimization loop

For the integration of the described procedure into an optimization loop, it is necessary to define an objective value. Since we need to find material parameter sets that are suitable for the utilization for accurate person individual simulation planning, a comparison between the simulation result of the standing position and the real skin surface of the volunteers taken from the 3-D scans is performed.

It is essential to bring the 3-D surface scan in best alignment with the simulation result in order to compute the

3-D displacement, formulated as the area integrated 3-D distance at each node of the FEA mesh. This leads to one single output parameter that can be interpreted as the correspondence between surface scan and FEA simulation result. Thus, it becomes possible to summarize the whole deviation into one value that needs to be minimized with the appropriate parameters for the mechanical behaviour. The whole process chain is visualized in figure 3.

As design variables that describe the mechanical behaviour of the soft tissue with Neo-Hookean material, Young's modulus and Poisson's ratio have been used that are inside the loop transformed to their hyper-elastic representations in initial shear modulus and initial bulk modulus.

For these particular optimizations the design space boundaries were set to be 0.39 - 1.17 kPa for the Young's modulus. This equals a variation of +/- 50 % in relation to a value from literature that has shown to be a fairly good first guess for the material stiffness. The second design parameter was the Poisson's ratio which has been varied in the scope of 0.3 to 0.5, meaning fully incompressible material behaviour.

Adaptive response surface method was used to optimally illuminate the design space and to draw maximal information about the overall system behavior out of the performed simulations.

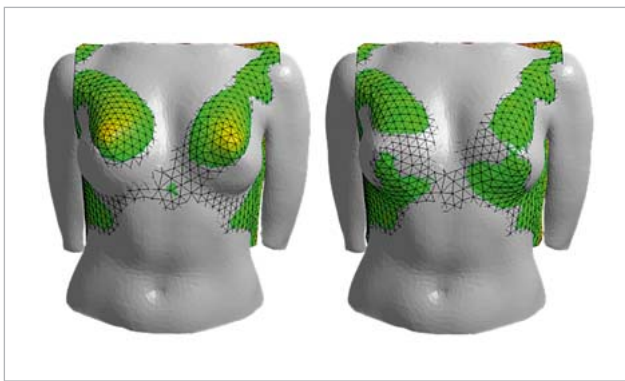


Fig. 4: Simulation results of the standing position with different material parameter sets: A much too stiff material behavior (left) and a more appropriate configuration (right). Deviations between the calculated standing position and the scanned 3-D surface visualized as color plots.

Results

The applicability of the presented workflow for the simulation of the breast could be shown. The whole process chain is automated and thus provides an easy to use interface for the validation of different material parameters. In figure 5, a typical result of an optimization run is shown. It is evi-

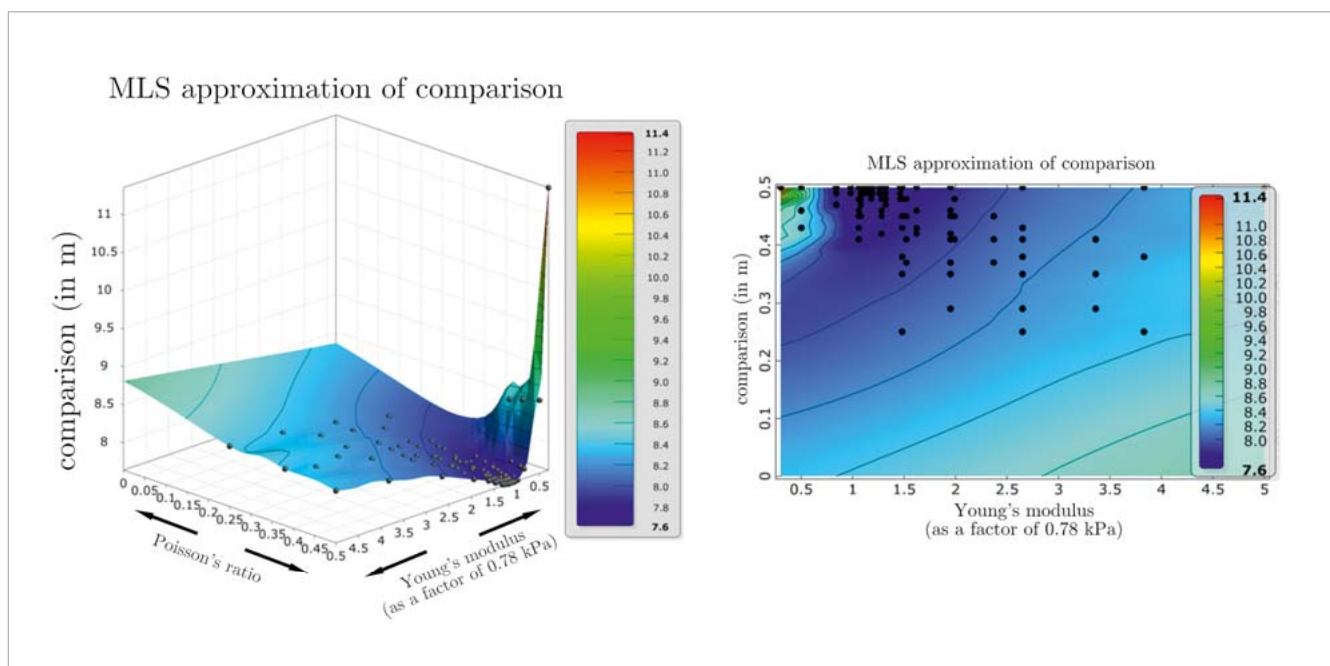


Fig. 5: Example of a response surface of an optimization with ARSM (adaptive response surface method). Young's modulus (E , factors to 0.13 kPa) and Poisson's ratio (ν) are plotted. Mean deviation between 3-D surface scan in standing position and FEA result in mm is shown as the height of the response surface as it is objective value that is to be minimized.

dent that there is a clearly defined optimum, i.e. the set of material parameters that is best suited to describe the real mechanical behaviour of the correspondent test person's breast. Looking first at the variations in Poisson's ratio, there is a decrease towards higher values, meaning less compress-

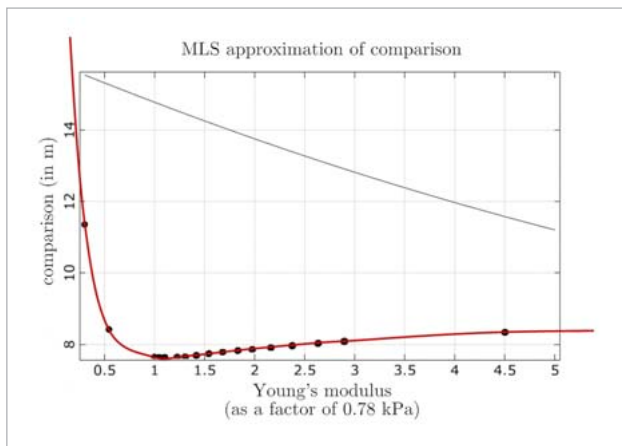


Fig. 6: Reduction of the design space to have only one free design variable which is the Young's modulus. The Poisson's ratio in this variant is fixed to full incompressibility. Then, clearly defined optima can be found as see by the red approximation curve.

ibility. Thus the commonly used assumption of biological soft tissues to be incompressible or at least nearly incompressible can be confirmed by these findings. Since this is true for all tested models, in future work it seems no more necessary to deal with compressible material models at all, resulting in the reduction of unknown material parameters.

Taking a further look at the material stiffness (figure 6), the Young's modulus, a clearly defined optimal position can be found. The model behaviour is described by a shallow slope when coming from high Young's moduli and a relatively steep increase when the material parameters become too soft. For all optimizations performed in the present study, defined global optima could be found. The individual optima for the eight test persons were found within the range of 0.494 kPa to 0.852 kPa for the Young's modulus. Hence, between the different test persons relatively high differences in soft tissue stiffness of 72.5% could be investigated, underlining the need for patient individual simulations.

Discussion

The advantage of the whole workflow presented here is the non-invasive character as a combination of volume imaging (MRI) and 3-D surface scanning (laser triangulation) and the involvement of the computer for the actual simulation. No tissue samples of the patient's soft tissue have to be harvested what is especially a critical issue if the mechanical information derived from these specimens should be used in operation planning, because this would mean an additional intervention for the patient. Furthermore, the expensive and cumbersome experimental testing can be circumvented.

The high variation in stiffness of almost a factor of 2 between the softest and the hardest optimal material parameter set found in this study shows the distinct need for the patient individual assessment of soft tissue material parameters. Thus patient specific simulations seem inevitable. Hence, the advantages of this non-invasive and fully computerized approach become obvious.

Outlook

The workflow presented in this publication may in the future be used for the material parameter assessment of hyper-elastic parameters that are suited for patient individual modelling of the constitutive behaviour of the female breast soft tissue. These data may subsequently be utilized for numerical simulations and planning of complex surgical interventions in plastic surgery.

The presented approach is not limited to its application in plastic surgery of the female breast. Other uses of this procedure for different body parts, e.g. for abdominal surgery or the simulations of soft tissue compression caused by prostheses in orthopedic treatments, are also possible but need to be further investigated. Besides these medical utilizations, there are also applications beyond that scope in other fields of science, e.g. in the determination of material properties of polymer components.

However, more complex models as the ones that have been used in the study presented here may in future be necessary when it comes to the application in breast surgery planning. For instance, more different anatomical regions such as the muscular soft tissue as well as a distinction of soft tissue into an adipose and a glandular compartment may yield more accurate anatomical models. These models may contain more tissues with unknown material properties, thus the dimensionality of the design space increases and hence the optimization task becomes more complex. Furthermore the influence of the modeling of the skin may have a decisive role, especially when the anisotropic material properties are considered. For these models, as well as for the use of more complex theoretical models such as Mooney-Rivlin or Ogden with more parameters than just stiffness and compressibility that can be varied, the benefit of the optimization software OptiSlang becomes instantly more pronounced.

Authors // S. Raith, M.Eder, A.Volf, L. Kovacs (Research Group CAPS (Computer Aided Plastic Surgery) - Klinik und Poliklinik für Plastische Chirurgie und Handchirurgie, Klinikum rechts der Isar, Technische Universität München)

J. Jalali (Institute of Medical Engineering at the Technische Universität München, IMETUM)

Source // www.dynardo.de/en/library



CASE STUDY // RAILWAY INDUSTRY

MODEL CALIBRATION OF A RAILWAY VEHICLE

With the help of optiSlang, calibration of a numerical model of Alfa Pendular train, including the car body, bogies and passenger-seat system, was conducted based on the natural frequencies and modal configurations estimated from dynamic tests.

Optimization task

When interacting with the railway track, moving trains induce vibrations that can affect the structural stability of the infrastructure, the stability of the track and of the wheel-rail contact and passengers' comfort. Complex models of the train-track coupled system are developed in order to perform an accurate analysis of the dynamic behaviour. In this type of models the modelling of the vehicles is conducted based on formulations grounded on the multi body dynamics and on formulations based on the finite-element method. In formulations based on the multi body dynamics, the car body, bogies and axles of the vehicles are modelled through rigid structures connected by springs and dampers which simulate the primary and secondary suspensions. In formulations based on the finite-element method it is possible to consider the deformability of the car body, bogies and axles. The development of these models requires the knowledge of the geometrical and mechanical parameters of the vehicle's structure.

The use of models which consider the deformability of the car body of the vehicle becomes more important due to the tendency to use increasingly lighter and slender structures

in the manufacture of trains to reduce weight and construction costs. It has been shown that the flexural vibration of the car body may contribute, in a large extent, to the accelerations that passengers are subjected to. The frequencies of these vibration modes range from 8.5 Hz to 13 Hz, which is significantly relevant regarding human beings' sensitivity to vibration.

This article describes the calibration of a numerical model of an Alfa Pendular train vehicle base on modal parameters. The modal parameters of the vehicle were determined based on a set of forced vibration tests that focused specifically on the car body, bogie and passenger-seat system. The calibration of the numerical model was conducted using a multistep approach involving two phases: the first phase concerned the calibration of the model of the bogie and the second phase focused on the calibration of the complete model of the vehicle. The calibration methodology involved a sensitivity analysis and an optimization. The global sensitivity analysis was based on a stochastic sampling technique and allowed the identification of the numerical parameters that most affect the modal responses

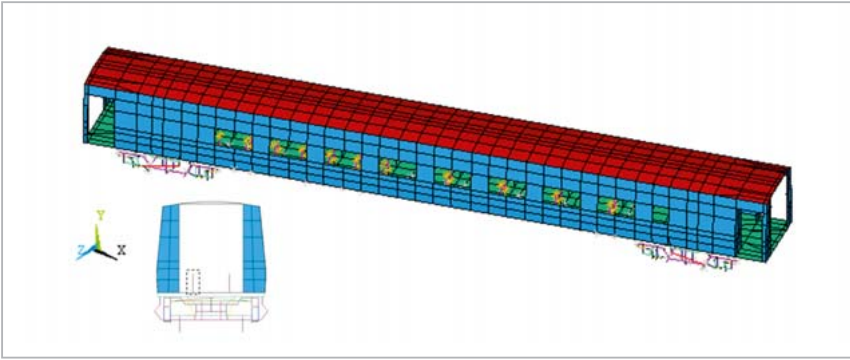


Fig. 1: Numerical model of the BBN vehicle

and, therefore, should be included in the optimization of the model. The optimization was carried out based on an iterative procedure using a genetic algorithm. A mode pairing criterion based on the modal strain energy using the Enhanced Modal Assurance Criterion (EMAC) was used to achieve the correct pairing of the numerical and experimental vibration modes. Finally, the modal parameters of the calibrated numerical model are compared with the modal parameters of the initial numerical model.

Numerical modelling

Description

The modal analysis of the BBN vehicle was performed using a three-dimensional finite element model developed in the ANSYS software. The use of a finite-element formulation allows considering the influence of the deformability of the car body, bogies and axles. Figure 1 presents a perspective of the numerical model. The car body was modelled by shell-finite elements while the bogies were modelled by beam-finite elements, with the exception of the suspensions, the connecting rods and the tilting system which were modelled by spring-damper assemblies. Additionally, the passenger-seat system was modelled, in a simplified manner, by a one-DOF system composed of a mass over a spring-damper assembly. The masses of the equipment located in the under-floor of the car body and bogies were simulated through mass elements. The structure was discretised with 1082 shell elements, 1029 beam elements and 148 spring-damper assemblies. The total number of nodes is 1902, corresponding to 10,704 degrees of freedom.

Car body

Table 1 presents the main geometric and mechanical parameters of the car body's numerical modelling, including the designation, the selected value, the unit and the bibliographic references that were used. Additionally, the characteristics of the statistical distribution of some of the parameters, later used in the calibration phase of the model are also shown. Figure 2 identifies the panels of finite elements considered in the numerical modelling of the car body in correspondence with the base, cover and side walls. In the

modelling of the side walls special attention was given to the positioning of openings corresponding to windows and access doors. The finite elements that simulate the various panels have length l and constant thickness e and are constituted by elastic and orthotropic materials. The thickness of each panel was determined based on the condition that the cross-sectional area of the

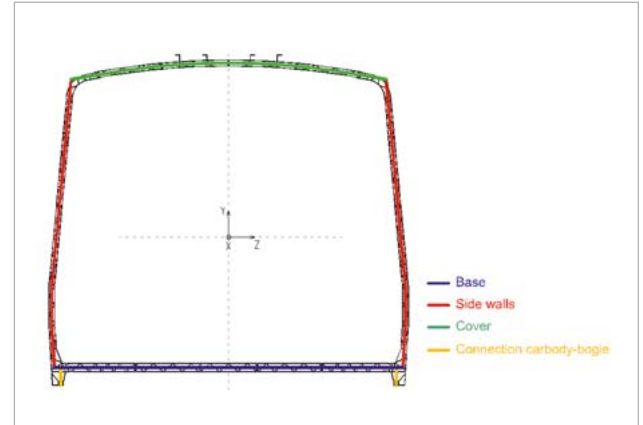


Fig. 2: Finite-elements panels from the numerical modelling of the carbody

finite-element panel is equal to the cross-sectional area of the real panel. The inertia correction of the panels, in directions x and z , was performed using the RMI parameter (Ratio of the bending Moment of Inertia):

$$RMI = \frac{I_{\text{real}}}{I_{\text{mod}}}$$

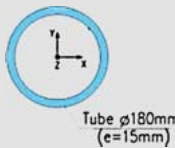
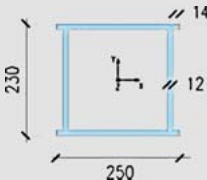
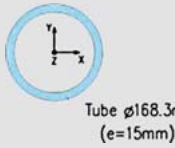
in which I_{real} is the real inertia of the panel and I_{mod} is the inertia calculated based on the thickness of the shell-finite element. The additional masses of the base, side walls and cover of the car body refer to the mass parcels of the item others under the component equipment and were uniformly distributed on the surface of the respective structural elements. The stiffness and damping parameters of the secondary suspension elements as well as their respective variation limits were estimated based on the values provided by the train's manufacturer.

Bogie

Figure 3 (see page 22) presents a perspective of the numerical model of the bogie. The chosen colours, combined with the legend, facilitate the identification of the different elements of the bogie. The beam elements connecting the wheel sets to the axle box have zero stiffness around their axle, so as to simulate the linkage with the axle box. The support conditions imposed on the bogie, particularly on

Parameter	Designation	Type	Statistical distribution		Adopted value	Unit	
			Average value/ standard deviation	Limits (lower/upper)			
K_{S1}	Stiffness of the vertical secondary suspension	Front bogie	Uniform	256.4/7.5	247/272.9	256.4	kN/m
K_{S2}		Rear bogie					
C_S	Vertical secondary suspension damping	Uniform	35/3.0	29.8/40.3	35	kN s/m	
C_{AL}	Yaw suspension damping	Uniform	400/34.6	340/460	400	kN s/m	
K_b	Stiffness of the tilting bolster-load bolster connection rod	Uniform	20,000/8660	5000/35,000	20,000	kN/m	
ρ_{alum}	Aluminium density	–	–/–	–/–	2700	kg/m ³	
E	Modulus of deformability of aluminium	–	–/–	–/–	70	GPa	
RMI_b	Corrective factor of the moment of inertia	Base	Uniform	225/101	50/400	90	–
RMI_p		Side walls	Uniform	90/34.6	30/150	114	–
RMI_c		Cover	Uniform	300/57.7	200/400	386	–
ΔMb	Additional mass	Base	Uniform	70/11.5	50/90	70	%
ΔMp		Side walls	Uniform	20/8.7	5/35	20	%
ΔMc		Cover	Uniform	7.5/4.3	0/15	10	%
e_{bas}	Equivalent thickness	Base	–	–/–	–/–	10.2	mm
e_{par}		Side walls	–	–/–	–/–	10.3	mm
e_{cob}		Cover	–	–/–	–/–	8.8	mm

Tab. 1: Characterisation of the main parameters of the numerical model of the carbody

Element	Cross-section	Geometrical characteristics
Axle		$A = 0.00778 \text{ m}^2$ $I_x = 0.267 \times 10^{-4} \text{ m}^4$ $I_y = 0.267 \times 10^{-4} \text{ m}^4$ $I_z = 0.534 \times 10^{-4} \text{ m}^4$
Girder (central zone)		$A = 0.01093 \text{ m}^2$ $I_x = 0.857 \times 10^{-4} \text{ m}^4$ $I_y = 0.887 \times 10^{-4} \text{ m}^4$ $I_z = 0.121 \times 10^{-3} \text{ m}^4$
Crossbar		$A = 0.00718 \text{ m}^2$ $I_x = 0.210 \times 10^{-4} \text{ m}^4$ $I_y = 0.210 \times 10^{-4} \text{ m}^4$ $I_z = 0.421 \times 10^{-4} \text{ m}^4$

Tab. 2: Geometric characteristics of the structural elements of the bogies

the girders and on the tilting and load bolsters, allow translational vertical movements and rotations around the x and z axes, preventing any other movements. Table 2 shows the geometrical characteristics of the sections of the various elements. The geometric characteristics are expressed in terms of the area (A) and inertias (I). Table 3 (see page 22) describes the main mechanical and geometrical parameters of the numerical model and the characteristics of the statistical distribution of certain parameters, which will be used in the model's calibration phase.

The stiffness and damping parameters of primary suspension elements and their respective variation limits were estimated based on information from the manufacturer. The additional mass of the bogie, at the girders, crossbars and axles, is related to the mass of springs, dampers, connecting rods, links, reinforcement plates, axle boxes and others. These masses were linearly distributed in the different elements. In what concerns the girders the additional mass was further divided into two parcels according to their location: in the central zone, i.e. in the sections located between the crossbars and at the extremities. The wheel–rail connection was modelled by a spring element with unidirectional behaviour.

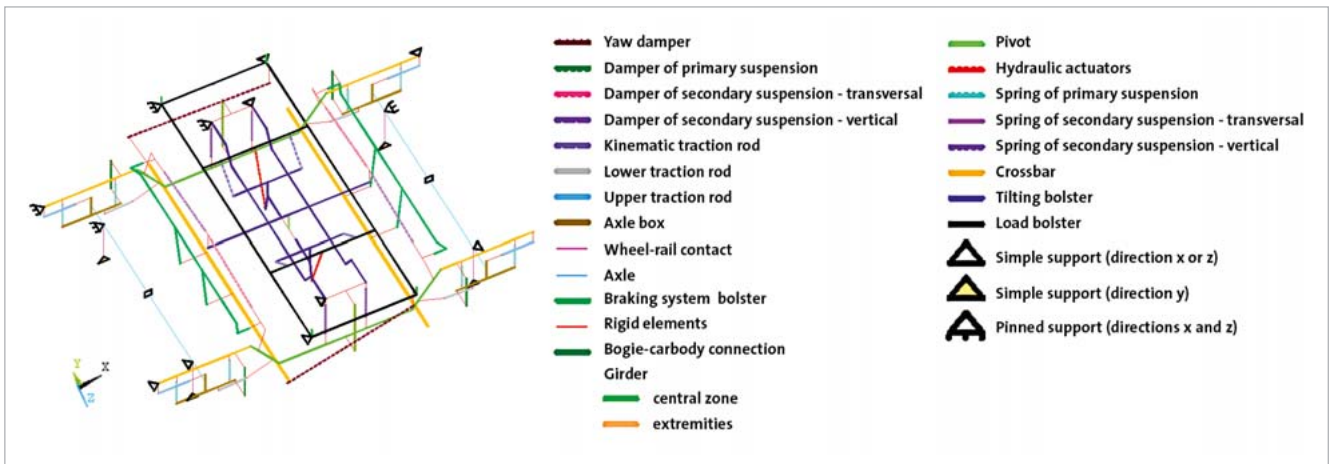


Fig. 3: Numerical model of the bogie

Parameter	Designation	Type	Statistical distribution		Adopted value	Unit	
			Average value/ standard deviation	Limits (lower/upper)			
K_p	Stiffness of the primary suspension	Uniform	564/26.6	518/610	564	kN/m	
c_p	Damping of the primary suspension	Uniform	18/1.6	15.3/20.7	18	kNs/m	
K_{bls}	Stiffness of the axle box connecting rods	Upper	6.5/0.8	5.2/7.8	6.5	MN/m	
K_{bli}		Lower	Uniform	25/2.9	20/30	25	MN/m
K_{rc}	Stiffness of the wheel-rail connection	-	-/-	-/-	1.5674×10^9	mN/m	
ΔMlc	Additional-mass	Girder (central area)	Uniform	75/43.3	0/150	42	kg/m
ΔMle		Girder (extremities)	Uniform	30/17.3	0/60	38	kg/m
ΔMt		Crossbar	Uniform	125/72.2	0/250	92	kg/m
ΔMe		Axles	-	-/-	-/-	271	kg/m

Tab. 3: Characterisation of the main parameters of the numerical model of the bogie

Element	Mode	Nature of vibration mode	Damped frequency (Hz)	Undamped frequency (Hz)	
Carbody	1C	Rigid body	Rolling	0.86	0.82
	2C		Bouncing	1.04	1.00
	3C		Pitching	1.42	1.33
	4C	Structural	First distortion	10.21	10.21
	5C		First bending	16.20	16.20
	6C		First torsion	15.05	15.03
Bogies	1B	Rigid body	Bouncing	8.21/8.18	6.57/6.26
	2B		Rolling	4.89/5.28	4.09/4.53
	3B		Pitching	12.10/12.04	9.50/9.41

Tab. 4: Numerical natural frequencies of the carbody and bogies

Modal parameters

Table 4 shows the damped and undamped natural frequencies of the main vibration modes of the BBN vehicle. In what concerns the bogies, for modes 1B and 2B, there are different frequency values according to the movement of the two bogies in phase and in antiphase, respectively. In the 3B mode, the different values of the frequencies are related to the isolated movements of the left and right bogies, respectively. The modal results show differences between damped and undamped natural frequencies. These differences are more notorious for the rigid body modes of the car body and bogies since these modes involve significant movements of the suspensions. In case of the bogies the differences are even more important since this additional damping is provided simultaneously by the primary and secondary suspensions. Figure 4 illustrates the modal configurations associated with rigid body modes (1C, 2C and 3C) and structural modes of distortion (4C), bending (5C) and torsion (6C) of the car body. In these modes the movements of the bogie have very low amplitude. Figure 5

shows the modal configurations, in perspective and cross-section view, of a bogie of the vehicle. Mode 1B comprises the bouncing movement of the bogie. Modes 2B and 3B comprise the rolling and pitching movements of the bogie, respectively. In these modes the car body shows very limited movements.

Calibration methodology

The results of the conducted experimental tests of the BBN vehicle involving the dynamic tests of the car body, bogie and passenger-seat system are used to calibrate the numerical model of the vehicle. The calibration of the numerical model of the BBN vehicle was performed using an iterative method based on an optimisation technique. This method consists on the resolution of an optimisation problem, which consists of the minimisation of an objective function by varying a set of the preselected model parameters. The pre selection of the numerical parameters is carried out based on a global sensitivity analysis. Figure 6 (see page 24) presents a flow-

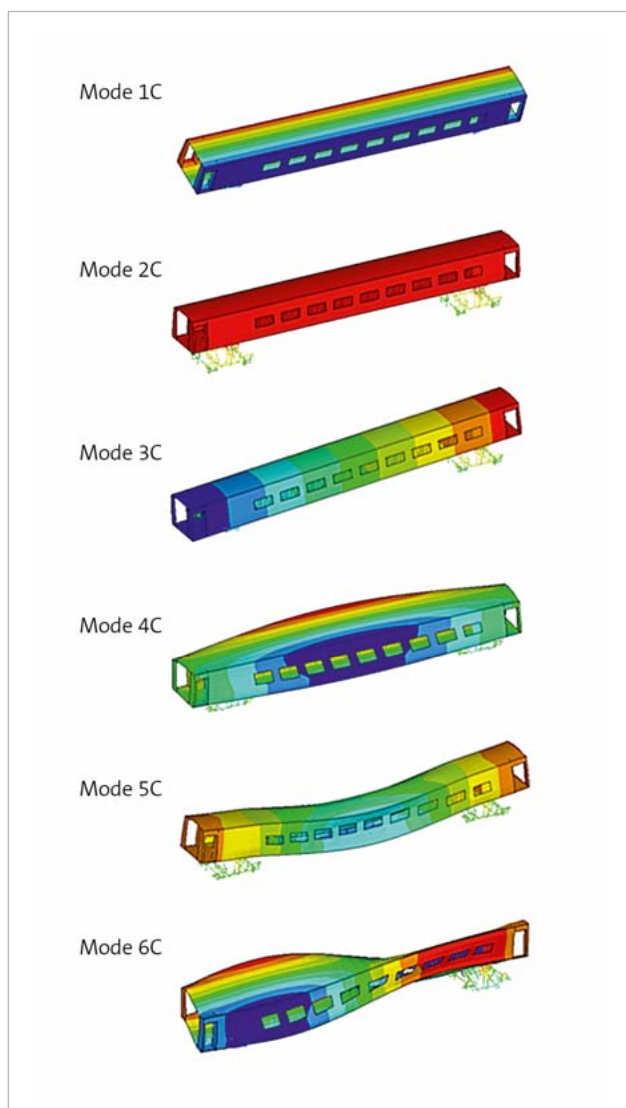


Fig. 4: Numerical rigid body and structural modes of vibration of the carbody

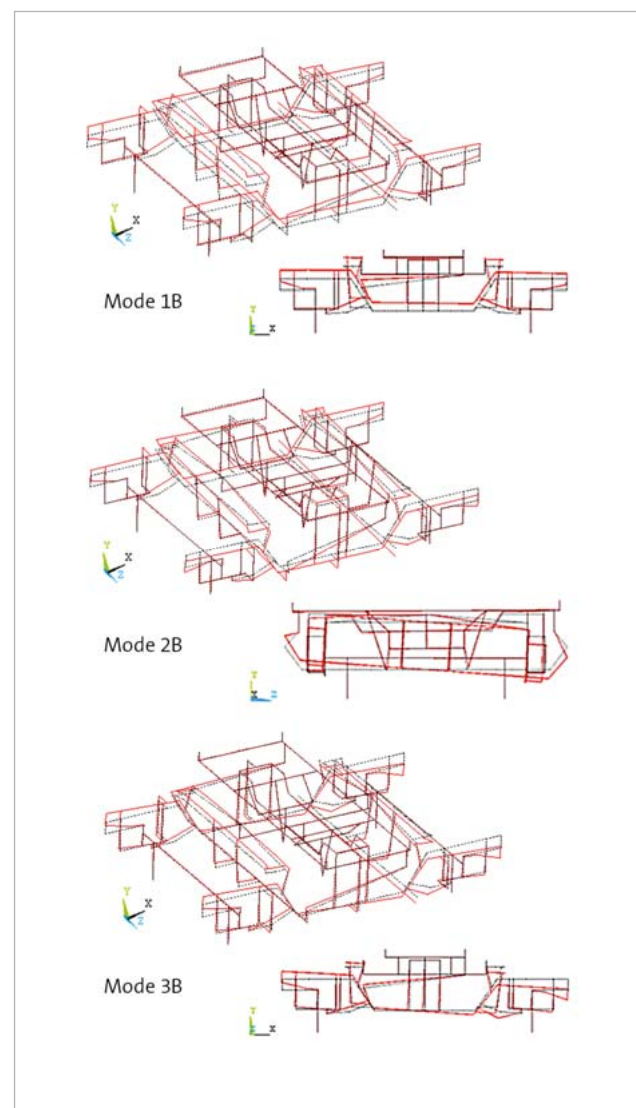


Fig. 5: Numerical modes of vibration of the bogies

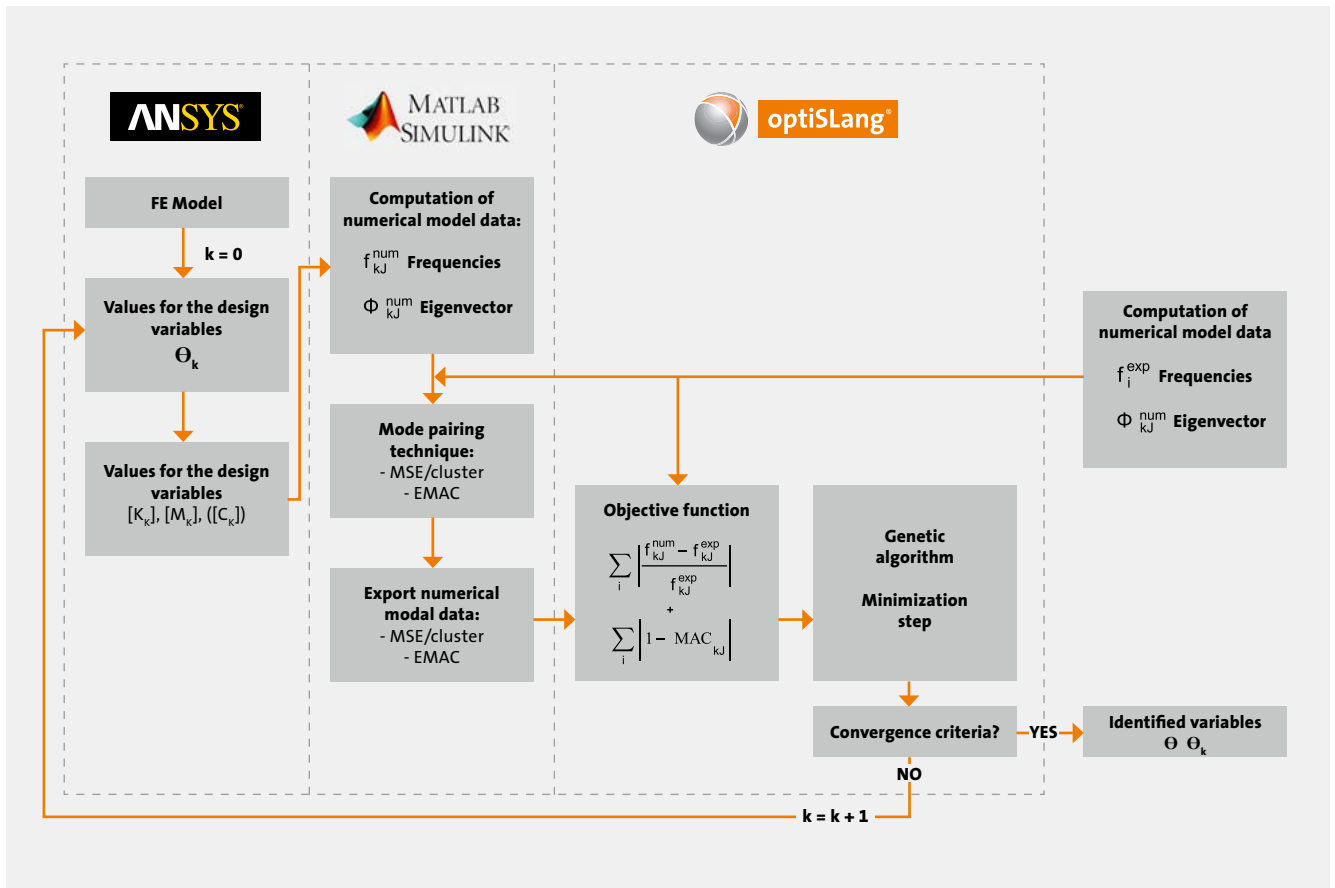


Fig. 6: Calibration methodology for the numerical model

chart illustrating the iterative method of calibration based on a genetic algorithm involving the use of three software tools: ANSYS, MATLAB and optiSLang. The main aspects of the implemented calibration methodology are described in reference. The calculation of modal parameters in systems with proportional damping matrix is based on a classic modal analysis [1]. In systems with non-proportional damping matrix the same calculation is based on a state-space formulation. The mode-pairing technique aims to establish a correspondence between experimental and numerical vibration modes. This task is often complex due to alterations in the order of the numerical modes, resulting from variations on the numerical parameters which occur during the optimisation process and also due to the limited number of degrees of freedom of experimental modes, which increases the number of possible correspondence between numerical and experimental modes. In this paper the correspondence between numerical and experimental modes is performed through an energetic criterion based on the modal strain energy and on the EMAC parameter. The objective function (f) is defined based on the differences between the numerical and experimental modal parameters [1]:

$$f = a \sum_{i=1}^n \frac{|f_i^{\text{exp}} - f_i^{\text{num}}|}{f_i^{\text{exp}}} + b \sum_{i=1}^n |\text{MAC}(\varphi_i^{\text{exp}}, \varphi_i^{\text{num}}) - 1|$$

where f_i^{exp} and f_i^{num} are the experimental and numerical frequencies referring to mode i , φ_i^{exp} and φ_i^{num} are the vectors containing the experimental and numerical modal information related to mode i , a and b are weighting factors of the objective function terms and n is the total number of vibration modes.

Calibration

The experimental calibration of the numerical model of the BBN vehicle was performed based on modal parameters which were identified by the dynamic tests of the bogie and car body. The first phase focused on the calibration of the numerical model of the bogie under test conditions [1]. The second phase focused on the calibration of the complete numerical model of the vehicle. The numerical parameters of the bogie estimated in the first phase were assumed as deterministic parameters in the second phase.

Calibration of the bogie

Numerical model under test conditions

The calibration of the numerical model of the bogie forced the development of a model that would reproduce the specific conditions of the test. Changes to the original model involved the removal of springs and dampers from the secondary sus-

Parameter	Designation	Type	Statistical distribution		Adopted value	Unit
			Average value/ standard deviation	Limits (lower/upper)		
K_b	Stiffness of the secondary suspension's elastic block Dir y^a	Uniform	12,000/1732	9000/15,000	12,000	kN/m
K_{btl}	Dir x and Dir z^a	Uniform	25,250/14,289	500/50,000	5000	kN/m
POS_{1e}	Position of the contact point of the actuation system Dir x^a Left side	Uniform	5/1.7	2/8	5	-
POS_{1d}	Right side					
POS_{2e}	Dir z^a Left side	Uniform	0/0.6	-1/1	0	-
POS_{2d}	Right side					
E_m	Modulus of deformability of wood	Uniform	8/2.3	4/12	10	GPa

Tab. 5: Characterisation of the parameters of the numerical model of the bogie under test conditions (^aAccording to the referential of Fig.: 8)

pensions and from the tilting and load bolsters. Elements were also added to simulate the interface between the bogie and the actuation system, including distribution blocks and elastic blocks of the secondary suspensions. Rigid supports were introduced, at the contact point of the hydraulic actuators, with the ability to assume different positions, thus meeting the deviations of the contact point in the longitudinal (x) and transverse (z) directions. The elastic blocks of the suspension were modelled by spring elements positioned in the vertical direction. The stiffness of the contact between distribution blocks and elastic blocks of the suspension was also modelled, in the x and z directions, through spring elements. Table 5 describes the mechanical and geometrical parameters of the numerical. These parameters should be considered together with the parameters indicated in Table 3.

The position of the contact point with the actuation system, in longitudinal and transverse directions, may assume different values for the left and right hydraulic actuators. The longitudinal position of the actuator was limited to positions 2–8.

Sensitivity analysis

Figure 7 shows the results of the global sensitivity analysis using Spearman's rank correlation coefficient. This sensitivity analysis was performed using a stochastic sampling technique based on 500 samples generated by the Latin Hypercube method. This analysis was based on the parameters intervals presented in Tables 3 and 5. The correlation coefficients between [-0.25, 0.25] were excluded from the graphical representation. The random generation of samples, particularly the parameters of the bogie's additional mass, was subject to the following restrictions:

$$-\epsilon \leq \Delta M - [L_{lc}\Delta M_{lc} + L_{le}\Delta M_{le} + L_l\Delta M_l] \leq \epsilon$$

where ΔM equals 842 kg, and L_{lc} , L_{le} and L_l represent the total length of the central area of the girders, the extremities of the girders and crossbars, equal to 4.46 m, 3.56 m and 5.26 m, respectively, and ϵ is a tolerance considered equal to 150 kg.

The correlation matrix shows that the stiffness of the primary suspensions, the additional mass of the girders (central area and extremities) and the stiffness of the lower traction rod of the axle box have significant influence over

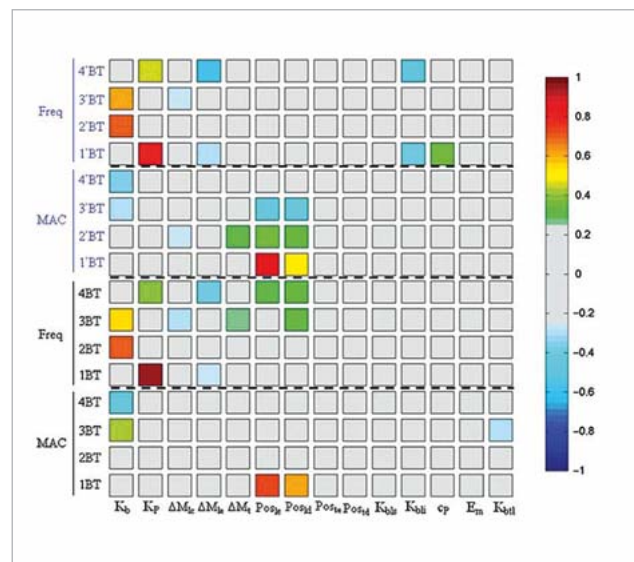


Fig. 7: Spearman's rank correlation coefficient between the parameters and responses of the numerical model of the bogie under test conditions

the vibration frequencies. In turn, the position of the actuators affects MAC values, particularly in modes 1BT. The vertical stiffness of the secondary suspension blocks influ-

ences the vibration frequencies and also the MAC values in a significant way. The remaining analysed parameters do not have significant influence on the modal responses and were therefore excluded from the optimisation phase. The influence of the primary suspensions' stiffness over the frequencies of modes 1BT and 4BT, for which the distance between the suspensions and the rotation axle of the bogie is larger, should be emphasised. In these modes the elastic block of the suspension has no influence over the responses due to its location near the rotation axle. It is not the case of the frequencies of modes 2BT and 3BT, which involve transverse translation and rotation of the bogie, respectively, and for which the stiffness of the suspension blocks, compared with the primary suspensions, is decisive for controlling the responses.

Optimisation

The optimisation of the model involved finally 10 numerical parameters and 16 modal results (8 vibration frequencies and 8 MAC values). The genetic algorithm was based on an initial population of 30 individuals considering 250 generations, in a total of 7500 individuals. The initial population was randomly generated by the Latin Hypercube method. A number of elites equal to 1 and a number of substitute individuals also equal to 1 have been defined in this algorithm. The crossover rate was assumed to be 50% and the mutation rate was considered equal to 15% with a standard deviation variable along the optimisation between 0.10 and 0.01.

The objective function is identical to that shown on page 24 considering a total number of vibration modes equal to 8 and weighting factors a and b equal to 1. The optimisation problem still includes restrictions related to the parameters of additional mass of the bogie. Optimal values of the parameters were obtained from the results of four independent optimisation cases (GB1–GB4) based on different initial populations. Figure 8 shows the ratios of the values of each parameter of the model in relation to the limits indicated in Tables 1, 3 and 5. The limits of the distributions of some of the parameters were extended, such as the cases of the stiffness of the primary suspension (500/1000 kN/m), and the stiffness of the axle box's traction rods (3/10 and 10/40MN/m) due to the systematic tendency of the optimum solutions of these parameters to reach the limits indicated in Table 3. A 0% ratio means that the parameter coincides with the lower limit. A ratio of 100% means that it coincides with the upper limit. The stiffness and damping parameters of the primary suspension and increments of mass are presented in Figure 8a indicating, in brackets, the numerical parameters' values.

The parameters related to the elastic elements (blocks and rod) and actuation system is shown in Figure 8b. The analysed parameters present a good stability with variations below 10%, except for the damping of the primary damper. This is one of the parameters that the sensitivity analysis has shown to have a smaller influence over the numerical

responses. Figure 9 summarises the error values between the numerical and experimental vibration frequencies, taking as reference the average values of the experimental frequencies, and the values of the MAC parameter, before and after calibration. The results after calibration are related to optimisation case GB2, which was the one presenting the lowest residual of the objective function. The average error of the frequencies decreased from 10.6% before calibration to 0.8% after calibration. In turn, the average value of the MAC parameter increased from 0.894 before calibration to 0.953 after calibration. As visualised in Figure 10, the experimentally obtained and numerically derived optimised modal configurations of the bogie coincide almost perfectly.

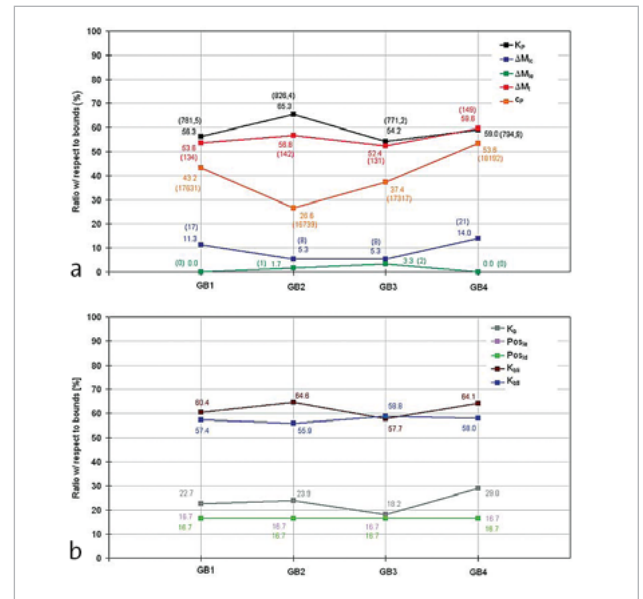


Fig. 8: Values of numerical parameters for optimisation cases GB1–GB4: (a) stiffness and damping of the primary suspension and increment of masses; (b) characteristics of the elastic elements and actuation system

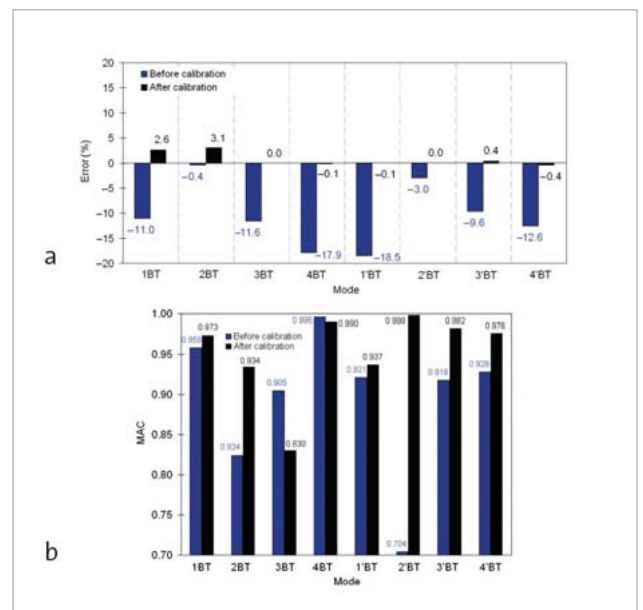


Fig. 9: Comparative analysis of the errors of experimental and numerical responses, before and after calibration: (a) vibration frequencies; (b) MAC

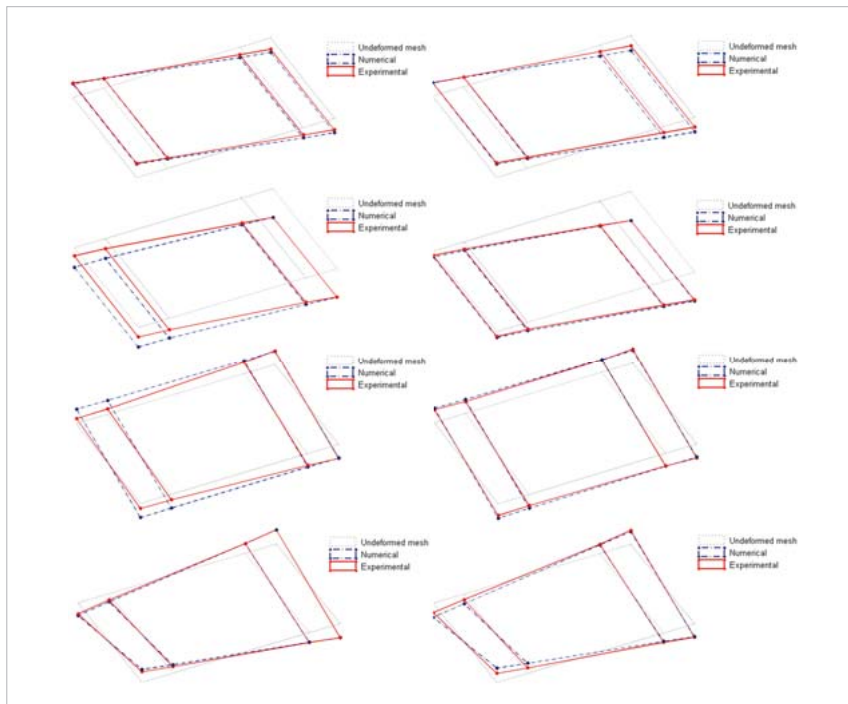


Fig. 10: Comparison between the experimental and numerical vibration modes of the bogie after calibration

Calibration of the complete model of the BBN vehicle

Sensitivity analysis

Figure 11 presents the results of the global sensitivity analysis using Spearman's rank correlation coefficient. The sensitivity analysis was performed using a stochastic sampling technique based on 250 samples generated by the Latin Hypercube method. This analysis was based on the parameters intervals presented in Table 2. The random generation of samples, particularly for the parameters of the car body's additional mass, was subject to the following restrictions:

$$-\varepsilon \leq \Delta M - [L_{lc}\Delta M_{lc} + L_{le}\Delta M_{le} + L_t\Delta M_t] \leq \varepsilon$$

where ΔM and L_t represent the additional mass on the base, side walls and cover, respectively, and ε is a tolerance equal to 10%. The mode pairing was performed by application of a technique based on the modal strain energy and on the EMAC parameter. The correlation matrix shows that the stiffness of secondary suspensions, from front (KS1) and rear (KS2) bogies, has significant influence over the frequencies and MAC values of the rigid body modes of the car body. In turn, the RMI parameters from the base (RMIb) and side walls (RMIp) essentially control the frequencies and MAC values of the structural modes of the car body. The parameters additional mass and stiffness of the connecting rod between the tilting and load bolsters (Kb) have significant influence over the vibration frequency of mode 1C. The remaining analysed parameters did not have significant influence with respect to the modal responses, and were consequently excluded from the optimisation phase.

It is possible to verify that the flexural stiffness of the side walls, which is controlled by the walls' RMI parameter, is important for controlling the torsional stiffness of the car body, as demonstrated by the high value of the correlation coefficient between the walls RMI parameter and the frequency of mode 4C.

Optimisation

The optimisation of the model finally involved 7 numerical parameters and 10 modal results (5 vibration frequencies and 5 MAC values). The control parameters of the genetic algorithm and the objective function are identical to those in the optimisation of the bogie. The optimisation problem also included constraints involving the car body's additional mass parameters. Optimal values of the parameters were obtained from the results of four independent optimisation cases

(GC1–GC4) based on different initial populations. Figure 12 (see page 28) shows the values' ratios of each parameter of the model in relation to the limits given in Table 1. The lower and upper stiffness limits of the secondary suspension were extended from 242 and 272.9 kN/m to 200 and 400 kN/m, respectively. Parameters related to the characteristics of the secondary suspension, connecting rod and geometrical properties of the car body are presented in Figure 12a indicating, in brackets, the estimated values for the stiffness of the secondary suspension. The parameters referring to mass distribution are presented in Figure 12b.

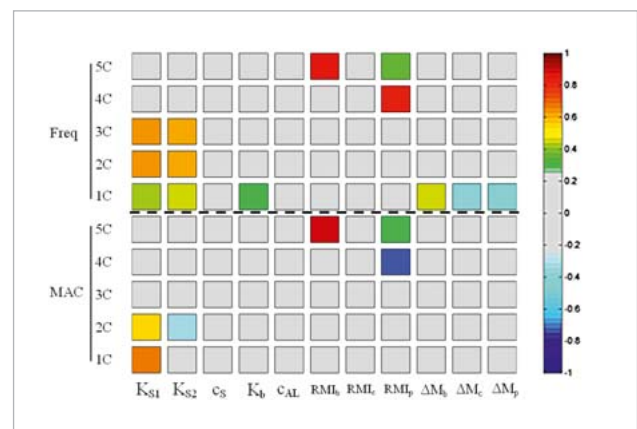


Fig. 11: Spearman's rank correlation coefficient between the parameters and responses of the carbody's numerical model

It is noticeable that the most stable parameters, with variations below 10%, are those that most affect the responses, including the stiffness of secondary suspensions and RMI

parameters of the base and side walls. The stiffness values of the front bogie's secondary suspension are higher than those estimated for the rear bogie. Regarding the additional masses of the side walls and cover, the estimates show higher variations, close to 25%. This should be related to the fact that these parameters contribute in a similar way to the participant mass on vibration mode 1C. Therefore, there may be different combinations of these parameters leading to the same solution, in terms of optimisation of the problem. Figure 13 summarises the error values of the numerical and experimental vibration frequencies taking as reference the average values of the experimental frequencies, and of the MAC parameter, before and after calibration. The results after calibration are related to the GC1 optimisation case, which was the one with the lowest final residual of the objective function. The frequencies' average error dropped from 20.3%, before calibration, to 2.9%, after calibration. This error decrease is mainly due to the reduction of the error associated with the frequencies of structural modes 4C and 5C. The average value of the MAC parameter did not change significantly, increasing from 0.927, before calibration, to 0.937, after calibration. The excellent agreement between the car body's experimentally obtained and numerically derived optimised modal configurations can be verified in Figure 14.

Final results

The combination between the numerical parameters, obtained for the optimisation case of the bogie GB2, and the parameters obtained in optimisation case of the complete vehicle GC1, were the basis for the establishment of the vehicle's calibrated numerical model. Table 7 presents the values of the damped vibration frequencies of the main vibration modes of the BBN vehicle obtained from the calibrated numerical model. Comparing the values of the frequencies with the values given in Table 4, concerning the initial numerical model, there is a visible tendency towards the frequency increase on the rigid body modes of the car body and bogies, being that, in the bogies' case, this increase ranged from 10% to 55%. This tendency is due to the significant increase of the stiffness of the primary and secondary suspension springs. In turn, the structural modes of the car body, particularly modes 4C and 5C showed a decreased tendency of approximately 20%, mainly due to the reduction of the RMI parameter of the car body's side walls.

Conclusions

This article described the calibration of the numerical model of a BBN vehicle of the Alfa Pendular train based on modal parameters. The calibration of the numerical model was conducted through an iterative methodology based on an optimisation algorithm and was performed using a multistep approach involving two phases: the first phase focused on the calibration of the model of the bogie under

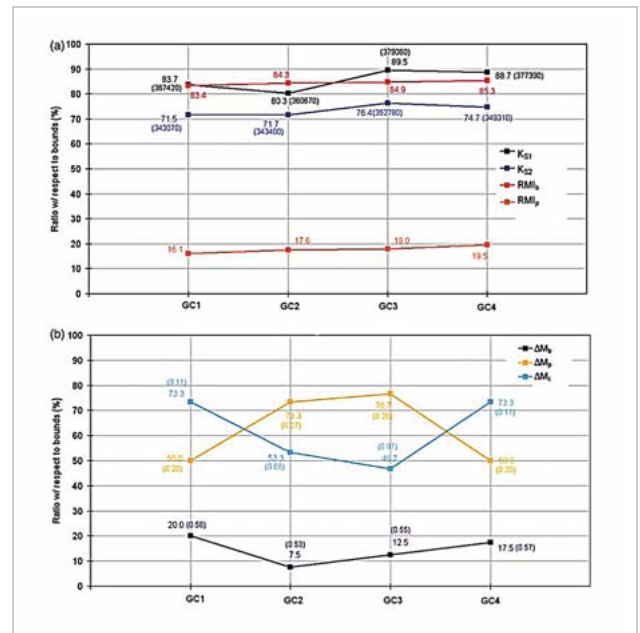


Fig. 12: Values of numerical parameters for optimisation cases GC1–GC4: (a) characteristics of the suspension, connecting rods and geometrical properties of the carbody; (b) masses

test conditions and the second focused on the calibration of the complete model of the vehicle. Global sensitivity analysis allowed the identification of numerical parameters to be considered in the calibration. The parameters that have shown the highest sensitivities in relation to the modal responses were, for the bogie, the vertical stiffness

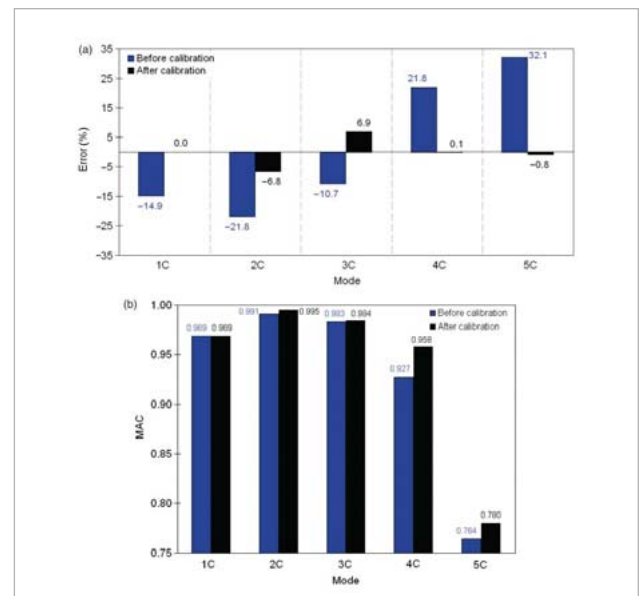


Fig. 13: Comparative analysis of the errors from the experimental and numerical responses, before and after calibration in terms of: (a) vibration frequencies; (b) MAC

of the secondary suspension block and the vertical stiffness of the primary suspensions. As for the car body, the RMI parameters of the base and side walls and the vertical stiffness of the secondary suspension were the parameters with highest sensitivity in relation to the modal responses.

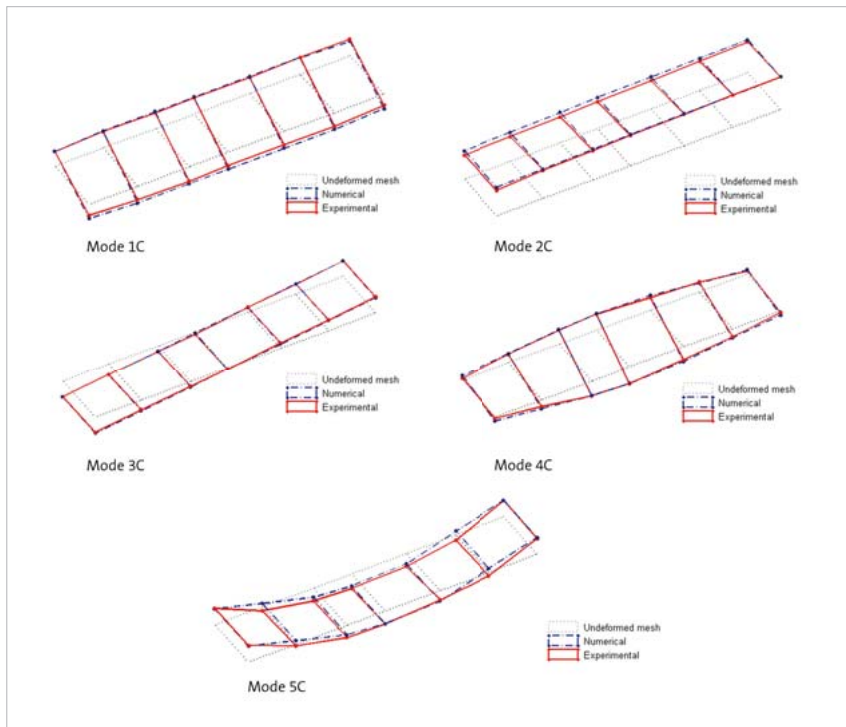


Fig. 14: Comparison between the vibration modes of the carbody, experimentally and numerically obtained, after calibration

The optimisation was conducted using a genetic algorithm involving a total of 17 numerical parameters and 26 modal responses. The results of the optimisation cases of the bogie and vehicle, based on different initial populations, led

Element	Mode	Damped frequency (Hz)
Carbody	1C	1.01
	2C	1.24
	3C	1.70
	4C	8.39
	5C	12.16
	6C	17.73
Bogies	1B	9.21/9.24
	2B	7.70/8.12
	3B	14.16/14.09

Tab. 7: Natural frequencies of the BBN vehicle obtained from the calibrated numerical model

mostly to very stable numerical parameters' values, particularly for those highly correlated with the responses. The comparison between the numerical vibration frequencies' values, before and after calibration, and the experimental vibration frequencies, has revealed significant improvements on the initial numerical models. The average error of vibration frequencies of the modes of the bogie under test conditions went from 10.6%, before calibration, to

0.8%, after calibration. Concerning the vibration modes of the complete model of the vehicle, the average error of frequencies went from 20.3%, before calibration, to 2.9% after calibration. Significant improvements were also observed in MAC values, particularly in the vibration modes of the bogie. This result demonstrates the robustness and efficiency of genetic algorithms on the estimation of the vehicle's modal responses. The combination of numerical parameters obtained for the GB2 bogie optimisation case with the parameters obtained for the GC1 case of vehicle optimisation provided the basis for developing the calibrated numerical model of BBN vehicle. Compared with the initial numerical model, the calibrated numerical models show higher frequency values of the rigid body modes of the car body and bogies, essentially due to the increased

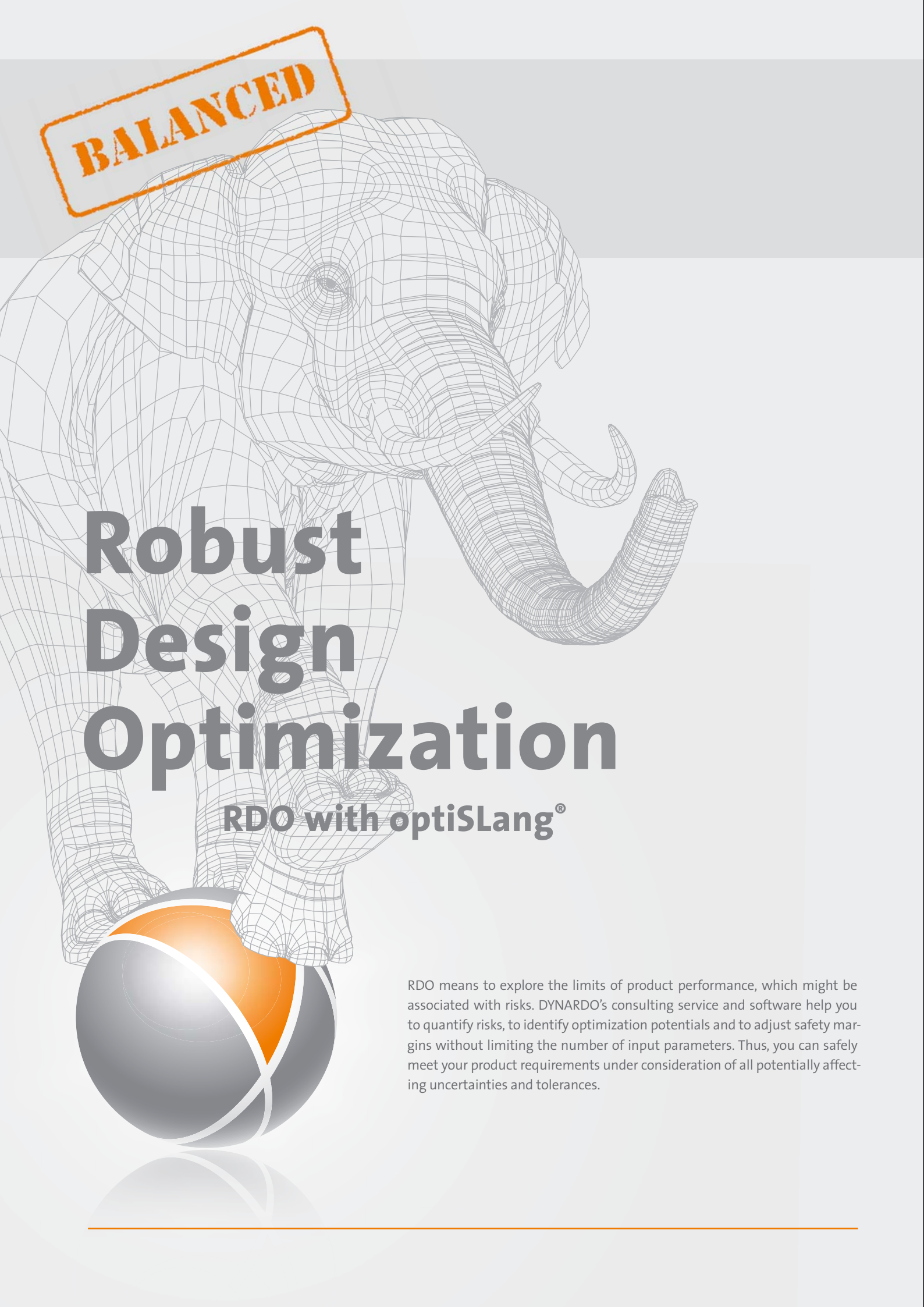
stiffness of the primary and secondary suspension springs. On the other hand, most of the car body's structural modes tended to decrease, largely due to a reduction of the RMI parameter of the side walls of the vehicle's car body. In future studies, the calibrated numerical model of the vehicle will be used to access the dynamic behaviour of the train-track coupled system, in terms of passengers comfort and wheel-rail contact stability, on plain track, on bridges or on transition zones.

Authors // D. Ribeiro (School of Engineering, Polytechnic of Porto) / R. Calçada, R. Delgado (Faculty of Engineering, University of Porto) / M. Brehm (BATir – Structural and Material Computational Mechanics, Université Libre de Bruxelles)/ V. Zabel (Bauhaus-University Weimar)

References // [1] D. Ribeiro, R. Calçada, R. Delgado, M. Brehm and V. Zabel (2013) - "Finite element model updating of a railway vehicle based on experimental modal parameters", *Vehicle System Dynamics*, 51 (6), pp. 821-856.

Source // www.dynardo.de/en/library

Title Image // Nuno Morão (© Wikimedia Commons)

A wireframe elephant is shown in profile, facing right. It is balancing a large, reflective ball on its trunk. The ball is split into two halves: the top half is orange and the bottom half is dark grey. The elephant's trunk is curved downwards, supporting the ball. The background is a light grey gradient.

BALANCED

Robust Design Optimization

RDO with optiSLang®

RDO means to explore the limits of product performance, which might be associated with risks. DYNARDO's consulting service and software help you to quantify risks, to identify optimization potentials and to adjust safety margins without limiting the number of input parameters. Thus, you can safely meet your product requirements under consideration of all potentially affecting uncertainties and tolerances.

METHOD OVERVIEW

Process automation and process integration

- Workflow definition via graphical user interface
- Reliable use with help of wizards
- Robust default settings for all algorithms
- Connection of arbitrary complex process chains
- Generate and use templates of process chains
- Parallelization and distribution of design evaluation
- Direct integration of Matlab, MS Excel, Python and SimulationX
- Supported connection of ANSYS, Abaqus, Adams, MADYMO
- Arbitrary connection of ASCII file interfaced solvers
- Full integration of optiSLang in ANSYS workbench
- Python interfaces to optiSLang algorithmic library
- Automatic generation and adaption of user flows via python scripting

Sensitivity analysis

- Classical Design of Experiments
- Advanced Latin Hypercube Sampling
- Correlation coefficients (linear, quadratic, rank-order)
- Principal Component Analysis
- Polynomial based Coefficient of Determination
- Polynomial based Coefficient of Importance
- Metamodel of Optimal Prognosis (MOP) with Coefficient of Prognosis (CoP)
- MOP/CoP based sensitivity indices for important variables

Multidisciplinary nonlinear optimization

- Continuous, discrete and binary design variables
- Gradient based optimization (NLPQL)
- Global Response Surface optimization using MOP with best design validation
- Adaptive Response Surface Method
- Evolutionary Algorithms (EA)
- Particle Swarm Optimization (PSO)
- Stochastic Design Improvement
- Multiobjective optimization using weighted objectives
- Multiobjective Pareto optimization with EA and PSO
- Start design import from previous samples

Parameter identification

- Parametrization and monitoring of response signals
- Signal function library including FFT, filtering etc.
- Sensitivity analysis using MOP/CoP to check identifiability
- Flexible definition of identification goal functions
- Local and global optimization methods to search for optimal parameters

Robustness evaluation

- Continuous and discrete random variables
- More than 20 probability distribution functions
- Distribution fits using measurements
- Correlated input variables using the Nataf model
- Monte Carlo and Advanced Latin Hypercube Sampling
- Statistical assessment of output variation including:
 - histograms with automated distribution fits
 - stochastic moments
 - quantile and sigma level estimation
- Sensitivity analysis with respect to random variables using correlations and MOP/CoP

Reliability analysis

- Definition of arbitrary limit states
- Monte Carlo and Latin Hypercube Sampling
- First Order Reliability Method (FORM)
- Importance Sampling Using Design Point (ISPUD)
- Directional Sampling
- Asymptotic Sampling
- Adaptive Response Surface Method

Robust Design Optimization (RDO)

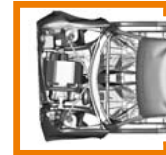
- Sequential and fully coupled procedures
- Variance based RDO
- Reliability based RDO
- Flexible definition of robustness measures using e.g. mean values, variances, Taguchi loss functions and probability of failure
- Consideration of robustness measures in optimization constraints and objectives functions

Post processing

- Statistic post processing including anthill plots, correlation plots and sensitivity indices
- Approximation post processing including 2D and 3D plots of response surfaces and the MOP
- Optimization post processing including Pareto frontier and convergence history of design variables, responses, objectives and constraints
- Show solver output images
- Parallel coordinates plot
- Traffic light plot
- Full interaction of single plots
- Design classification using coloring, selection/deselection
- High quality outputs in BMP, PNG, SVG, EPS and PDF format

CONSULTING, SUPPORT, TRAININGS

DYNARDO's consulting team has extensive expertise in the application of CAE-based analysis and Robust Design Optimization in the fields of structural mechanics and dynamics. At seminars and events, we provide basic or expert knowledge of our software products and inform about methods and current issues in the CAE sector.



CAE-Consulting

The DYNARDO GmbH offers individual calculation and simulation services in various fields of industries, e.g. consumer goods industry, mechanical and process engineering, energy industry, civil engineering, geomechanics, automotive industry, aerospace industry, bioengineering and micromechanics. We give support in all phases of product development: from the first predevelopment and feasibility studies over sensitivity analysis up to the development of the optimal design by robustness evaluation and reliability analysis. Due to the company's combination of software development and consulting, we achieve a high amount of flexibility referring to special market requirements in the CAE sector.

Support

The main interest of our support team is a successful customer. We provide technical support by phone, e-mail or online. All requests regarding our software products optiSLang, multiPlas, SoS and ETK will be processed thoroughly and answered immediately. Our support team will also help you to implement efficient RDO applications and its various methods to solve CAE-challenges in your particular field of business.

Free information days and webinars

With our free info days and webinars, you can get an introduction to performing complex, non-linear FEM calculations using optiSLang, multiPlas, SoS and ETK.

Simulation in civil engineering and geomechanics

The participant will get an introduction of advanced simulation options in combination with the finite element programs ANSYS and LS-DYNA. Information will be given about comfortable 3D modeling, particularly for complex structural geometries in linear or nonlinear structural mechanics, in structural dynamics or in multi-physics simulation.

Robust Design Optimization (RDO) with optiSLang and optiSLang inside ANSYS Workbench

This event provides an overview of optimization techniques and appropriate stochastic methods of robustness evaluation with optiSLang inside ANSYS Workbench. Practical examples will show how the software components are used to investigate a design space systematically, to determine sensitivities, to perform optimizations with competing goals and to consider the effect of scatter influences.

Trainings

For a competent and customized introduction to optiSLang, visit our basic or expert trainings explaining clearly theory and application of sensitivity analysis, multidisciplinary optimization, robustness evaluation and Robust Design Optimization (RDO). The trainings are not only for engineers, but are also perfectly suited for decision makers in the CAE-based simulation field. For all trainings there is a discount of 50% for students and 30% for university members/PHDs. You can find an overview of the current training program at our homepage.

Internet library

Our internet library is the perfect source for your research on CAE-topics and practical examples of CAE-based Robust Design Optimization (RDO). There you will find state-of-the-art information matched to the different fields of methods and applications.

Infos //

www.dynardo.de/en/consulting

www.dynardo.de/en/trainings

www.dynardo.de/en/library

Contact & Distributors

Germany & worldwide

Dynardo GmbH
Steubenstraße 25
99423 Weimar
Phone: +49 (0)3643 9008-30
Fax.: +49 (0)3643 9008-39
www.dynardo.de
contact@dynardo.de

Dynardo Austria GmbH
Office Vienna
Wagenseilgasse 14
1120 Vienna
www.dynardo.at
contact@dynardo.at

Germany

CADFEM GmbH
Marktplatz 2
85567 Grafing b. München
www.cadfem.de

science + computing ag
Hagellocher Weg 73
72070 Tübingen
www.science-computing.de

Austria

CADFEM (Austria) GmbH
Wagenseilgasse 14
1120 Wien
www.cadfem.at

Switzerland

CADFEM (Suisse) AG
Wittenwilerstrasse 25
8355 Aadorf
www.cadfem.ch

Czech Republic, Slovakia, Hungary

SVS FEM s.r.o.
Škrochova 3886/42
615 00 Brno-Židenice
www.svsfem.cz

Sweden, Denmark, Finland, Norway

EDR & Medeso AB
Lysgränd 1
SE-721 30 Västerås
www.medeso.se

United Kingdom of Great Britain and Northern Ireland

IDAC Ltd
Airport House Business Centre
Purley Way
Croydon, Surrey, CR0 0XZ
www.idac.co.uk

Ireland

CADFEM Ireland Ltd
18 Windsor Place
Lower Pembroke Street
Dublin 2
www.cadfemireland.com

Turkey

FIGES A.S.
Teknopark Istanbul
Teknopark Bulvarı 1 / 5A-101-102
34912 Pendik-Istanbul
www.figes.com.tr

North Africa

CADFEM Afrique du Nord s.a.r.l.
Technopôle de Sousse
TUN-4002 Sousse
www.cadfem-an.com

Russia

CADFEM CIS
Suzdalskaya 46, Office 203
111672 Moscow
www.cadfem-cis.ru

India

CADFEM Engineering Services India
6-3-902/A, 2nd Floor, Right Wing
Rajbhawan Road, Somajiguda
Hyderabad 500 082
www.cadfem.in

USA

CADFEM Americas, Inc.
27600 Farmington Road, Suite 203 B
Farmington Hills, MI 48334
www.cadfem-americas.com

Ozen Engineering Inc.
1210 E Arques Ave 207
Sunnyvale, CA 94085
www.ozeninc.com

USA/Canada

SimuTech Group Inc.
1800 Brighton Henrietta Town Line Rd.
Rochester, NY 14623
www.simutechgroup.com

Japan

TECOSIM Japan Limited
4F Mimura K2 Bldg. 1-10-17
Kami-kizaki, Urawa-ku, Saitama-shi
Saitama 330-0071
www.tecosim.co.jp

Korea

TaeSung S&E Inc.
Kolon Digital Tower 2
10F, Seongsu-dong 2 ga
Seongdong-gu
Seoul 333-140
www.tsne.co.kr

China

PERA-CADFEM Consulting Inc.
Bldg CN08, LEGEND-TOWN
Advanced Business Park,
No. 1 BalizhuangDongli,
Chaoyang District,
Beijing 100025
www.peraglobal.com

Imprint

Publisher

DYNARDO GmbH
Steubenstraße 25
99423 Weimar
Germany
www.dynardo.de
contact@dynardo.de

Executive Editor & Layout

Henning Schwarz
henning.schwarz@dynardo.de

Registration

Local court Jena: HRB 111784

VAT Registration Number

DE 214626029

Publication

Worldwide

Images

S.19, Nuno Morão (Wikimedia Commons)

Copyright

© 2013 DYNARDO GmbH. All rights reserved.
The DYNARDO GmbH does not guarantee or warrant accuracy or completeness of the material contained in this publication.